

Direct and indirect electrification of chemical industry using methanol production as a case study

Chao Chen^a, Yangsiyu Lu^{b,c}, Rene Banares-Alcantara^{a,*}

^a Department of Engineering Science, University of Oxford, Parks Road, Oxford OX1 3PJ, UK

^b Institute for New Economic Thinking, University of Oxford, Walton Well Road, Oxford OX2 6ED, UK

^c Smith School of Enterprise and the Environment, University of Oxford, South Parks Road, Oxford OX1 3QY, UK

HIGHLIGHTS

- Evaluation of direct and indirect electrification of methanol production.
- Direct electrification implemented through stand-alone heat-pumps.
- Indirect electrification implemented by substituting fossil based feedstock.
- Indirect electrification has great environmental and economic potential.
- Carbon dioxide abatement can reach up to 1.35 kg/kgMeOH if electricity is 100% green.

ARTICLE INFO

Keywords:

Electrification of chemical industry
Methanol
Carbon dioxide utilisation
Techno-economic models
Heat pumps
Pinch technology

ABSTRACT

This work aims to explore the electrification of chemical industry taking the production of methanol as a case study. A reference process, with a basis of 400,000 tonne per annum, is first simulated in Aspen Plus to produce methanol via traditional natural gas reforming. As an indirect electrification strategy, a non-conventional carbon dioxide hydrogenation methanol plant is then designed to substitute fossil fuel feedstock. Standalone heat-pumps are implemented as a direct electrification method in both processes at various extents generating different scenarios. It has been found that direct electrification has a small impact on energy consumption in all scenarios. In the reference process, direct electrification can only substitute 7.1 MW of heating, accounting for 7.8% of the total heating. In contrast, the energy structure of the indirectly electrified process is completely changed from the reference process: (1) very high temperature heating is eliminated; (2) electricity consumption is increased from 14.2 to 604.1 MW due to feedstock (hydrogen) synthesis. The renewable energy penetration and electricity price are taken into consideration when financial and environmental assessments are performed. At approximately 88% of renewable penetration, carbon neutrality is achieved in the indirectly electrified process. The net present value of the indirectly electrified process breaks even at an electricity price of 22 €/MWh and exceeds its counterpart reference process at 3–4 €/MWh. This analysis will enable the integration and management of renewable energy for methanol production and will facilitate future studies on the electrification of chemical production.

1. Introduction

The environmental impact of chemical production has drawn significant attention and reduction in greenhouse gas (GHG) emissions has been called for to mitigate climate change. Currently, chemical industry is mostly powered by the combustion of fossil fuels, which is responsible for a significant portion of anthropogenic GHG emissions. To tackle climate change the necessity of electrification has been agreed

and understood by many energy experts [1], but it seems to be contradictory to conventional wisdom: electricity generation and transmission involve substantial energy losses and thus its application as a heat source in chemical industry is less efficient than onsite combustion from an energy efficiency point of view. However, the potential of electrification mainly lies in a future scenario where there is a pathway leading to zero-carbon electricity. In fact, more than two decades ago, the importance of electrification was noted as an economical way to

* Corresponding author.

E-mail address: rene.banares@eng.ox.ac.uk (R. Banares-Alcantara).

Nomenclature	
APEA	Aspen Process Economic Analyser
CapEx	capital expenditures (€)
CEPCI	chemical engineering plant cost index
COP	coefficient of performance
COP_{eff}	effective coefficient of performance
CR	combined reforming
C_t	cash flow of year t (€)
DMFC	direct methanol fuel cell
DR	dry reforming
E	activation energy in MEA/ CO_2 reactions (MJ/mol)
E_a	activation energy in MeOH synthesis (J/mol)
F	flowrate (kmol/h)
FC_p	aggregated heat capacity (kJ/K)
f	fraction (mol%)
GCC	grand composite curve
GHG	greenhouse gas
HHV	high heating value
HP	heat-pump or high pressure
IRR	internal rate of return
k	pre-exponential factor
LHHW	Langmuir-Hinshelwood-Hougen-Watson
LP	low pressure
M	M module, $M = (\text{H}_2 - \text{CO}_2)/(\text{CO} + \text{CO}_2)$
MEA	monoethanolamine
MEACOO^-	carbamate monoethanolamine
MEA^+	protonated monoethanolamine
MeOH	methanol
MP	medium pressure
NG	natural gas
NLP	non-linear programming
NPV	net present value (€)
P	pressure (bar or atm)
OpEx	operational expenditures (€)
\dot{Q}	rate of heat or enthalpy change (kW)
r	discount rate
R	ideal gas constant (J/mol K)
RES	renewable energy source
RWGS	reverse water-gas-shift
SR	steam reforming
T	temperature (°C or K)
TFCC	total fixed capital cost (€)
TR	tri-reforming
VHP	very high pressure
\dot{W}	rate of mechanical work (kW)
WGS	water-gas-shift
η	efficiency of refrigeration cycle
η_c	carbon efficiency
η_e	energy efficiency

reduce the reliance on carbon-based energy [2].

The use of renewable energy sources (RES) plays a pivotal role in electrification and yet poses a significant challenge: the intermittency and variability of RES impact the stability of the grid and require improved planning and coordination to accommodate the fluctuations in availability. To this end, there are solutions underway, particularly in electricity market rules, design and operation [3]. Besides the technology aspects, policy formulation also poses additional difficulties. For instance, when energy reliability, often a top priority, is taken into account, the penetration of RES may be impeded. In addition, many public policies stress energy efficiency, which may be an inadequate metric to evaluate the energy structure as it misses the environmental benefits of electrification. Therefore, a targeted and farsighted policy will be required to drive a wholesale transition of fossil fuel to electricity-based heating (or any other energy utility) [4]. Although there are many problems to be addressed in electrification, a broad consensus of pathways towards clean electricity exists. The same may not yet be said of fossil fuel combustion even with highly efficient technologies. Biofuels, as an alternative to fossil fuels, may lead to reduced carbon emissions (this is questioned when land-use change is taken into account [5]), but they have proven less favourable in economic potential and scalability [6]. For this and other reasons, consensus is growing that electrification may be required to meet GHG reduction goals.

There are many types of electrification that can be implemented in current chemical industry. Kranenburg and co-workers proposed a Power-to-X scheme in their white paper to categorise the electrification into four types [7]. However, we would like to simplify the categorisation to direct and indirect electrification: direct use of electricity in a chemical process to provide heating and mechanical work or indirect use to synthesise alternative feedstock with higher energy content. This is justified by the fact that fossil fuel dependency is determined by its energy and/or feedstock requirements [8]; however, it is impossible to substitute fossil based feedstock with electricity. Many chemicals, such as ethylene, propylene and aromatics, are produced from crude oil or other complex organic molecules. Without a substantial innovation, fossil based feedstock will continue to play a vital role in chemical production. On the other hand, hydrogen (H_2) from electrolysis has demonstrated a great promise for the energy transition. In conjunction

with CO_2 capture and air separation technologies, energy vectors such as methanol (MeOH) and ammonia (NH_3) can be synthesised, paving the way to zero-carbon industry in the future. In addition to chemical production through hydrogenation, routes such as direct electro- [9] and photo-catalytic [10] reactions to synthesise chemicals also represent highly electrified processes. However, they are excluded from our proposed electrification scheme due to scalability and economic feasibility. Regarding direct electrification for process heating, the simple replacement of heating using electricity is inefficient and thus we focus on the implementation of heat-pumps to facilitate process heat integration. The implementation of heat pumps requires minimum modification to current industrial processes, as opposed to the indirect electrification scheme. Therefore, to explore the potential of electricity in chemical production, an analysis of direct and indirect electrification schemes is proposed.

The idea of direct hydrogenation is not new and has been largely demonstrated in MeOH synthesis. The Bouallou group proposed a conceptual design to produce MeOH from CO_2 hydrogenation [11]. In light of this work, the Perez-Fortes group evaluated the performance of such a plant based on environmental and economic metrics. The groups of Deng & Adams [12] and Bukhtiyarova [13] also investigated the production of MeOH from high CO_2 content sources. In a very recent work, the Wessling group reported CO_2 hydrogenation to produce MeOH with an innovative process layout [14]. This idea also holds great potential for a large variety of chemicals [15] and appears the most promising synthetic application [16]. All of these works focus on carbon capture and utilisation and specific catalytic reactions, but lack a holistic view of chemical process electrification and its implications, i.e. alternative electrification options are not considered and the energy structure of an electrified process remains unexplored. This gap prevents or at best inhibits the introduction of RES in MeOH production (or any other chemical processes) as the current designs are not scoped for electrification. The Harnisch group reported electrification of biotechnical systems and analysed its economic potential [17]; however this work is hardly applicable to the wide chemical industry. In a recent study, Nayak-Luke et al. have demonstrated the design of “green” NH_3 production powered by RES [8], and quantified the requirement of RES storage for a fully electrified process [18]. Such a concept for MeOH

production is still missing at present. However, to consider the utilisation of RES the electricity and/or energy consumption at the process level is required. The importance of electrification and fuel switching has been demonstrated in end-use sectors [19] but very few studies have focused on the impact of electrification from a chemical process perspective. As commented by the Lechtenbohmer group, the future scenario of a fully electrified system is an area with several knowledge gaps where the potential for the electrification of chemical industry requires more knowledge regarding technology and system options [20]. Therefore, it is imperative to explore the electrification schemes at a process level to identify their opportunities as well as potential barriers. Table 1 summarises the scope of previous studies as well as their limitations with regard to chemical industry electrification. The aims of this work are to provide technological options and strategies for chemical process electrification, and analyse process performance based on environmental and economic metrics. Concretely, we investigate MeOH production as a case study to evaluate the impact of electrification on process design by proposing alternative technological scenarios generated from different electrification schemes. Understanding of the energy structure of the electrified process is also key because such an analysis is a first step before introducing RES in chemicals production, as the optimisation of RES scheduling, sizing and storage require an insight of the fully (or almost fully) electrified process. We hope this work can build a foundation for the use of RES as well as provide insights for policymaking in terms of future electricity demand.

2. Methods

This work aims to probe the potential of chemical production processes electrification and investigates the MeOH production process as a case study. To this end, we have proposed a conventional MeOH synthesis route through natural gas reforming as a reference process. The electrification is considered at two levels: (1) direct electrification by heat-pump implementation, and (2) indirect electrification using an alternative feedstock or intermediate that can be produced from electrolysis. In particular, MeOH synthesis through CO₂ hydrogenation is simulated as an indirectly electrified process. The direct electrification does not alter the process design but it changes the energy structure of the process, i.e. substituting thermal energy with electricity. On the contrary, the use of alternative feedstocks may substantially change the flowsheet of the design. Therefore, to make a sound comparison it is of

particular importance to define the boundary of the assessment. In this work, both the energy consumption of the production processes and the utilities associated with feedstock production are considered. However, the price of electricity is considered as an exogenous factor and detail about electricity generation from renewable sources is outside the scope of this work. Detailed assumptions are listed at the end of this section.

The MeOH production processes are simulated with the commercial software Aspen Plus V9 at a basis of 400,000 tonne per annum with a product purity of 99.8 wt%. The carbon capture from flue gas is modelled as a chemical absorption process using a MEA solution. Water electrolysis is not simulated but it is integrated in the performance analysis since its energy consumption is readily available from published literature. The viability of electrification is assessed based on economic and environmental analyses.

2.1. Water electrolysis unit

The production of H₂ is typically achieved through alkaline electrolysis that splits water into oxygen and hydrogen [28]. This process essentially stores electrical energy as chemical energy in the form of H₂ [29], and thus it is of significance in the electrification of chemical processes. The system efficiency of commercial electrolyzers ranges from 56% to 73% or 70.1 to 53.4 kWh/kg H₂ at 1 atm and 25 °C [30].

Since the water electrolysis process produces hydrogen and oxygen simultaneously, it would be correct to allocate the energy consumption to both products. However, to make a sound comparison between electrification schemes, a cryogenic air separation process (the traditional method to produce commercial oxygen) was simulated but is not shown in this work. The simulation resulted in an electricity consumption of approximately 1 kWh/kg O₂, which is much lower than for the aforementioned water electrolysis process (70.1–53.4 kWh/kg H₂). Therefore, it is a fair approximation to allocate all the energy consumed in electrolysis to the H₂ product. In this work, an energy consumption of 4.5 kWh/Nm³ H₂ is assumed [31] in a water electrolysis process. This is equivalent to 55.7 kWh/kg H₂ at the feed conditions of the simulated process.

2.2. Carbon capture simulation

The feedstock CO₂ used in natural gas dry reforming and CO₂ hydrogenation is captured from the flue gases of a pulverised coal power

Table 1

Summary for previous studies and their limitations with regard to chemical industry electrification.

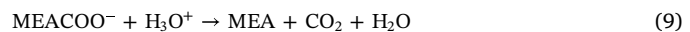
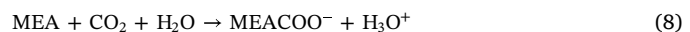
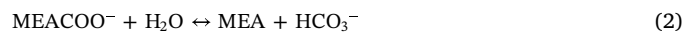
Previous studies	Contributions	Limitations
Charoensuppanimit, et al. [21]	■ proposed CO ₂ hydrogenation for MeOH with H ₂ from a side-reaction	■ no implications for electrification
Van-Dal and Bouallou, [11]; Alsayegh, et al. [14]; Perez-Fortes, et al. [22]	■ proposed conceptual designs of hydrogenation plants with H ₂ from electrolysis ■ can potentially achieve energy transition and reduce the reliance on fossil fuel based feedstock	■ energy structure reported but not from the electrification perspective ■ not scoped for electrification, i.e. other electrification schemes are not considered
Ren, et al. [23]; Chen, et al. [24]; Temvuttiroj, et al. [25]	■ generalised the hydrogenation process to other chemicals ■ enhanced the potential of hydrogenation in chemical industry electrification	■ only focused on catalytic reaction ■ analysis at a process level is missing ■ energy structures are not reported ■ not scoped for electrification, i.e. other electrification schemes are not considered
Zhao, et al. [10]; Cheng, et al. [26]	■ proposed alternative process for hydrogenation ■ demonstrated a potential in reduction of fossil fuel dependency	■ the considerations cannot be applied to other chemical production ■ analysis at a process level is missing
Harnisch, et al. [17]	■ chemical synthesis through electricity-driven bio-production	■ its impact on the industrial sector is analysed as a whole ■ analysis at a process level is missing ■ no electrification schemes are provided for chemical industry
Ebrahimi, et al. [19]	■ demonstrated the importance of electrification and fuel switching ■ focused on regional end-use	
Khanna, et al. [27]	■ reported strategies in decarbonisation by electrification and RES adoption	

plant with an overall recovery of 80%. The simulation flowsheet adopted in this work was originally proposed by Aspen Technology, Inc. in an example of the rate-based MEA absorption process, thus the physical properties models in Aspen Plus are also inherited from the original design (the key physical property prediction model for vapour-liquid equilibrium is ENRTL-RK, i.e. an electrolyte NRTL activity coefficient model for the liquid phase and the Redlich-Kwong equation of state model for the vapour [32]). Nevertheless, modifications were made in the absorber that models the WASH unit as a two-stage packed column (see Fig. 1). Li et al. also simulated a CO₂ capture process based on the same example with improvements in temperature adjustments mapping their experimental results [33]. In this work, the temperature adjustments that account for heat losses are neglected for the sake of simplicity.

Fig. 1 shows the carbon capture process through MEA absorption and regeneration. After desulfurisation, the flue gas is fed to the bottom of the absorber whereas the lean CO₂ MEA solvent is fed to the top of the column. The scrubbed gas is then introduced at the top of a washing column in order to minimise the waste of MEA. Both columns are modelled with a RADFRAC unit using a rate-based model (RADFRAC is a model that performs rigorous calculations involving stage-by-stage vapour-liquid equilibrium coupled with chemical reactions. This model can also be used in rating or design mode [34]). Regarding the internals, both columns are designed as packed columns with 20 and 2 stages, respectively. The rich solvent from the bottom of the absorber is fed to the desorber to recover CO₂ and MEA. The desorber is also modelled with RADFRAC as a reactive distillation column. A partial condenser is employed to dehydrate CO₂ at a fixed temperature of 18.0 °C with a reflux ratio of 0.58. Since the operating temperature is below the temperature of cooling water, refrigeration is required to chill the condenser. The reboiler of the desorber is designed to have a boilup ratio of 0.06 operating at 119.3 °C. After regeneration, the lean solution is mixed with a small fraction of the water stream from the washing section and then re-injected into the absorber. The carbon capture unit has embedded a heat exchanger to recover heat from the MEA regeneration, this exchanger is included in the plant-wide heat integration to minimise energy utilities.

The chemistry of the absorber and the stripper consists of five instantaneous reactions (Reactions (1)–(5)) and 4 finite rate reactions

(Reactions (6)–(9)).

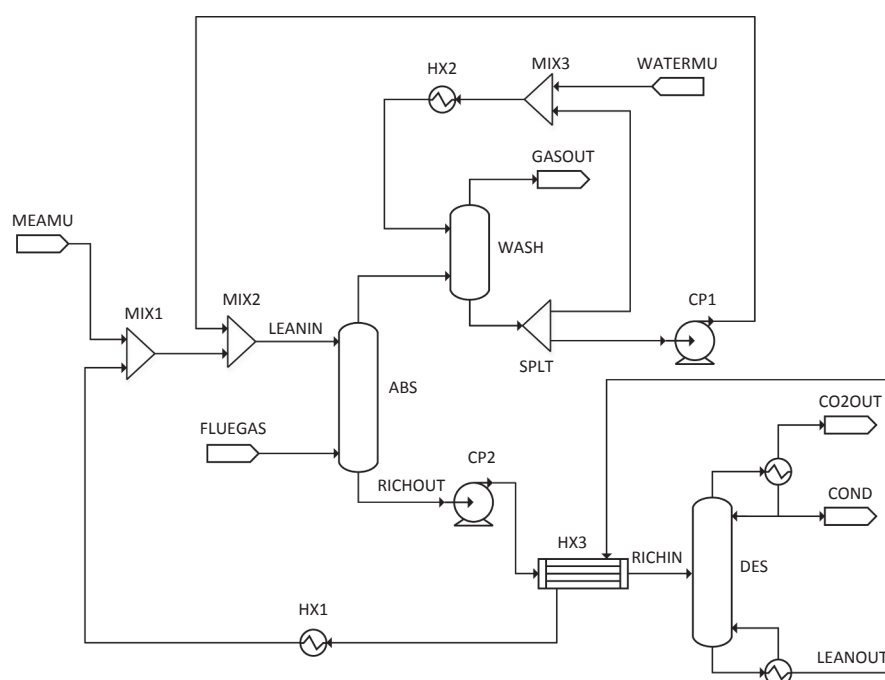


The equilibrium parameters for Reactions (1)–(5) are computed from the Gibbs free energies. Regarding the rate-controlled reactions, built-in power law equations were used. The pre-exponential factor (*k*) and activation energy (*E*) of Reactions (6)–(9) are tabulated in Table 2 and entered in Aspen Plus [35]. Note that the kinetic parameters are the same in the absorber and desorber unless otherwise specified.

The captured CO₂ from the unit has a purity of 99.4 wt% with impurities such as H₂O and N₂. For simplicity, the impurities are neglected when the stream is fed to the downstream MeOH production process. Due to the specification of the condenser operation, the captured CO₂ is chilled at a temperature (18 °C) lower than ambient; however the heating duty to bring CO₂ to ambient temperature is neglected since the

Table 2
Pre-exponential factor (*k*) and activation energy (*E*) in the rate-controlled reactions. Data are obtained and rearranged from Ref. [35].

Reaction	<i>k</i>	<i>E</i> (MJ/mol)
(6)	1.33e + 17	55.5
(7)	6.63e + 16	107.4
(8)	3.02e + 14	41.3
(9) absorber	5.52e + 23	69.2
(9) desorber	6.50e + 27	95.4



STREAM
FLUEGAS = flue gas where CO₂ is extracted
MEA MU = make up of MEA
WATER MU = make up of water
LEAN IN = stream lean in CO₂ fed to ABS
RICH OUT = stream rich in CO₂ from ABS
RICH IN = stream rich in CO₂ fed to DES
LEAN OUT = stream lean in CO₂ from DES
GAS OUT = waste gas
CO₂ OUT = captured CO₂
COND = condensate water

UNIT
SPLT = splitter
MIX*i* = *i*th mixer
HX*i* = *i*th heat exchanger/cooling/heater
CP*i* = *i*th compressor/pump
ABS = absorber column
DES = desorber column
WASH = washing tower

Fig. 1. Process flow diagram of the carbon capture unit based on MEA absorption.

Table 3

Composition of the flue gas in the carbon capture unit. Data are obtained from Ref. [32].

Component	wt%
H ₂ O	7.1
CO ₂	8.5
N ₂	74.3
O ₂	10.1

value is insignificant. At the condenser, it is assumed that the vapour product is cooled to 40 °C by cooling water, and chilled further to 18 °C by refrigeration. The mechanical power (kW) required to run the refrigeration cycle is calculated by

$$\dot{W} = \dot{Q} \left(\frac{T^H}{T^L} - 1 \right) \frac{1}{\eta} \quad (10)$$

where \dot{Q} (kW) is the rate of heat extracted or the enthalpy change per unit of time of the process stream from 40 to 18 °C, T^H (308.15 K) is the temperature at which heat is rejected to a heat sink, T^L (281.15 K) is the temperature at which heat is extracted from a heat source and η is the efficiency of the refrigeration process which is assumed to be 50%.

The flue gas is assumed to be free of charge and pre-treated before carbon capture, and its composition is shown in Table 3. For simplicity, the carbon capture process is only simulated at the same scale as the example in [32], which was adopted in our work; thus the energy

utilities are linearly scaled up in the plant-wide integration.

2.3. MeOH production simulation

In the reference process MeOH is produced with syngas from natural gas reforming. The overall process is illustrated in Fig. 2. The production process is composed of three main sections: (1) nature gas reforming, (2) MeOH synthesis and (3) MeOH distillation process. To simplify the chemistry of the reforming process, natural gas is assumed to be pure methane; in the simulation the trace amounts of N₂, H₂S, heavy alkanes (C2 and above) and other rare gases are neglected. In the first section of the flowsheet CH₄ is compressed and fed to the reformer to produce syngas, which is a mixture with varying proportions of H₂ and CO. Traditionally syngas is produced from the steam reforming (SR) of natural gas through a catalytic process to obtain a high H₂/CO ratio. An alternative process to produce syngas is through CO₂ reforming (also known as dry reforming, DR, as opposed to steam reforming, SR) of natural gas. Although this method has many disadvantages, including a low H₂/CO ratio in the produced syngas and coke formation due to large C/O ratio, it has drawn focus over the last decade due to its potential to use CO₂ as a feedstock. In addition, reports have indicated that there are many natural gas fields having high CO₂ content (up to 30%) all over the world (such as natural gas reservoirs in Indonesia's Natuna [36], Malaysia in general [37] and Colorado Plateau [38]). Developments in catalytic systems such as Rh supported on Al₂O₃ [39], Mo₂C on ZrO₂ [40] and Ni-Ce on Al₂O₃ [41] have also facilitated the application of the DR process. However, in the

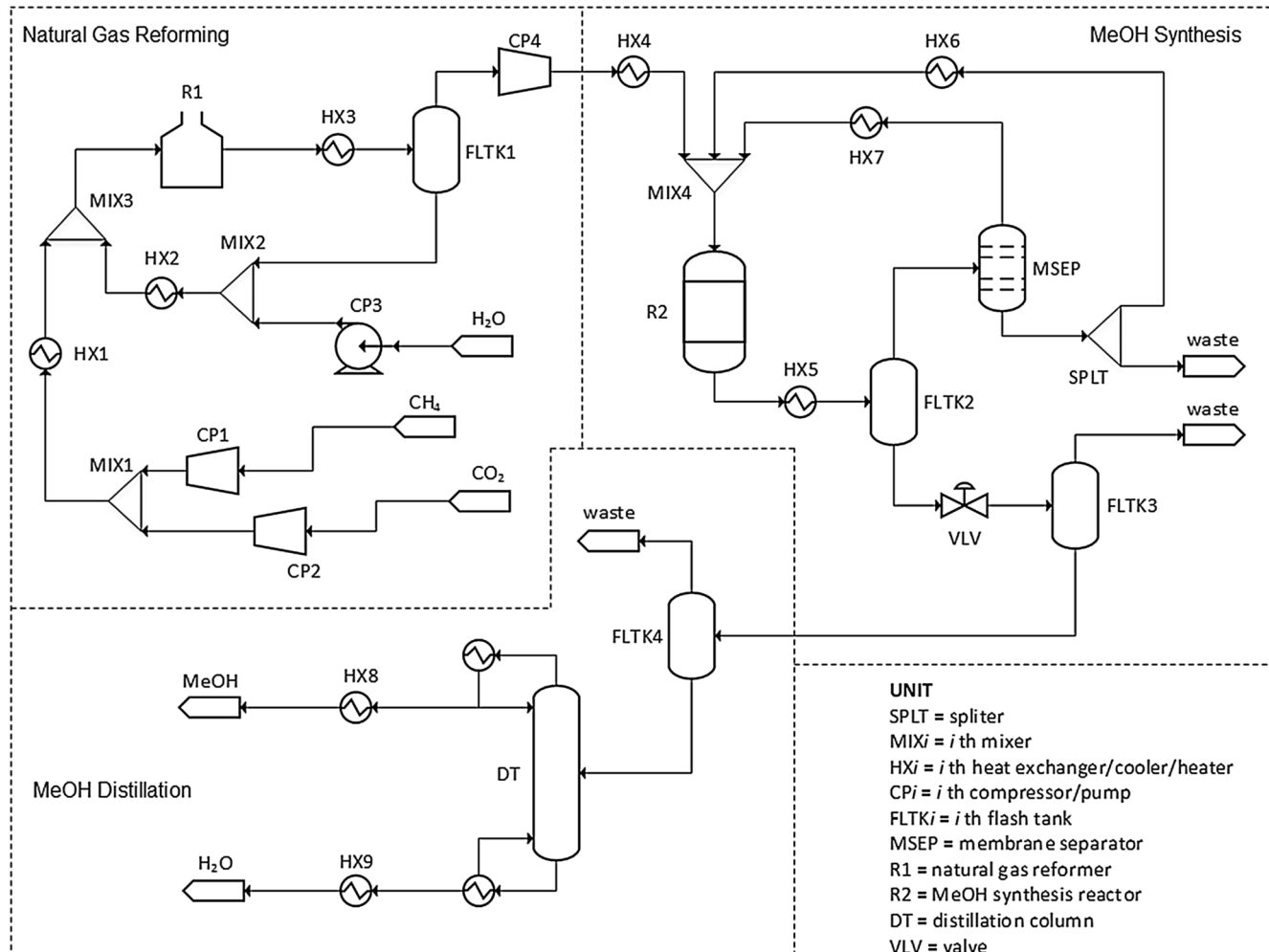


Fig. 2. Process flow diagram of the reference MeOH production plant simulated in Aspen Plus.

base case scenario of this work, the CO₂ input to the reforming processes is from a carbon capture process rather than from natural gas. Another motivation to feed CO₂ in the reformer is because the downstream MeOH synthesis loop generates a surplus of low-grade heat (relative to the natural gas reforming process) which can be integrated in the CO₂ capture process.

Despite the promising future of DR, we would like to restrain ourselves to a more conservative process to reform natural gas since the aim of this work is to assess the electrification based on current industrial technologies. Consequently, we formulate the natural gas reforming process based on the work of Olah et al. [42] and Canete et al. [43], which proposed a combined reforming (CR) process consisting of DR (Reaction (11)) and SR (Reaction (12)). The water-gas-shift (WGS) reaction also occurs (Reaction (13)) in the reformer, however this reaction is not independent as it can be obtained from a linear combination of DR and SR. It is also noteworthy that the Boudouard reaction and the methane decomposition reaction have been neglected due to the fact that minimum formation of coke has been found in the thermodynamic analysis [44].



As shown in the process flowsheet, water is fed to the reformer (unit R1 in Fig. 2) to enable the SR and WGS reactions. From a thermodynamic analysis [44], it has been found that the yield of carbon dramatically decreases with respect to the increase of H₂O/CH₄ ratio and it reaches zero when H₂O/CH₄ ratio is 0.7 or above. Furthermore, the ratio of H₂/CO is directly proportional to the H₂O/CH₄ ratio due to the facilitated WGS reaction. The major drawback of a high H₂O/CH₄ ratio is the low conversion of CO₂, which implies a requirement for CO₂ removal at the downstream processes. Moreover, the high water content also incurs additional energy consumption and thus higher operating cost. As a compromise, the H₂O/CH₄ ratio is set to be approximately 2.0 in order to maximise the H₂/CO ratio in the product while the conversion of CO₂ is adequate enough to avoid its removal downstream.

The gaseous product and unreacted water are separated in a flash tank. The syngas product is fed to the MeOH synthesis loop whereas water is recycled back to the reformer. The reformer is modelled with a REQUAL reactor operating at 950 °C and 20 bar. Reaction temperature is determined through a sensitivity test in order to obtain optimal H₂/CO ratio and *M* module (defined as *M* = (H₂ – CO₂)/(CO + CO₂)) whilst keeping high CH₄ conversion. Details of product flowrate and design parameters at different reformer temperatures can be found in Figs. 10 and 11 in Appendix A. For simplicity, a perfect separation of gas and liquid is assumed in the syngas flash tank [11], and thus it is modelled with a SEP separator (FLTK1 in Fig. 2) in Aspen Plus. Nevertheless, the subsequent vapour-liquid separations are modelled with a rigorous flash drum.

The second section of the production flowsheet addresses the synthesis of MeOH from syngas through hydrogenation. Although there is a lack of consensus around the involved reactions, we propose a simplified set of reactions including the hydrogenation of CO (Reaction (14)) and CO₂ (Reaction (15)), and the reverse water-gas-shift (RWGS) reaction (Reaction (16)) that co-occurs with the MeOH conversion. Other reactions that produce by-products are neglected, which is in accordance with other reports (the work of Van-Dal and Bouallou [11] and Perez-Fortes et al. [22]). This results in a stoichiometric H/C ratio of 2.5. As a rule of thumb, the CO₂/CO ratio is limited to 0.5 to prevent the formation of water and catalyst deactivation [45]. MeOH synthesis typically requires a high H₂/CO ratio of up to 3.5 in the feed syngas; as a comparison, this ratio is approximately 1.0 for dimethyl ether production and 2.0 for gas-to-liquid processes [40].



In industry, the MeOH synthesis loop is often composed of a series of adiabatic reactors with inter-stage cooling. The economic removal of the heat generated in the MeOH synthesis is a separate study and a major challenge in the design for MeOH production [46]. Therefore, to simplify the process, the MeOH reactor is modelled as a single RPLUG reactor (unit R2 in Fig. 2) in Aspen Plus operating at constant temperature and pressure of 255 °C and 71 bar. The kinetic model implemented in this work is based on that of a commercial Cu/ZnO/Al₂O₃ catalyst proposed by Bussche and Froment [47] with adjusted parameters [48]. The rate equations for Reactions (15) and (16) are rearranged to suit the requirements of the LHHW (Langmuir-Hinshelwood-Hougen-Watson) kinetic model in Aspen Plus [11]. Eqs. (17) and (18) represent the reaction rate of the MeOH synthesis and RWGS reaction respectively, wherein the kinetic constants are derived from the Arrhenius law in Eq. (19). The pre-exponential constants and activation energy terms are rearranged in Eqs. (20) – (22) and their values are summarised in Table 4. It is worthy to note that the thermodynamic equilibrium constants of Reactions (15) and (16) are rearranged and incorporated into the kinetic constants *k*₆ and *k*₇ respectively and thus they are not shown explicitly. The NRTL-RK physical properties method is employed (due to its capability to model non-ideal behaviour) to calculate the thermodynamic properties in MeOH synthesis [49]. The product composition at the corresponding reactor volume is illustrated in Fig. 12 in Appendix A.

$$r_{\text{MeOH}} = \frac{k_1 P_{\text{CO}_2} P_{\text{H}_2} - k_6 P_{\text{H}_2\text{O}} P_{\text{MeOH}} P_{\text{H}_2}^{-2}}{(1 + k_2 P_{\text{H}_2\text{O}} P_{\text{H}_2}^{-1} + k_3 P_{\text{H}_2}^{0.5} + k_4 P_{\text{H}_2\text{O}})^3} \left[\frac{\text{mol}}{\text{kg}_{\text{cat}} \text{s}} \right] \quad (17)$$

$$r_{\text{RWGS}} = \frac{k_5 P_{\text{CO}_2} - k_7 P_{\text{H}_2\text{O}} P_{\text{CO}} P_{\text{H}_2}^{-1}}{1 + k_2 P_{\text{H}_2\text{O}} P_{\text{H}_2}^{-1} + k_3 P_{\text{H}_2}^{0.5} + k_4 P_{\text{H}_2\text{O}}} \left[\frac{\text{mol}}{\text{kg}_{\text{cat}} \text{s}} \right] \quad (18)$$

$$k_i = K_i e^{-\frac{E_{ai}}{RT}} \quad (19)$$

$$\ln k_i = A_i + \frac{B_i}{T} \quad (20)$$

$$A_i = \ln K_i \quad (21)$$

$$B_i = -\frac{E_{ai}}{R} \quad (22)$$

Because of the equilibrium limitations, the synthesis of MeOH through hydrogenation requires a large excess of H₂. The unreacted gas is first separated from the liquid product and then undergoes a polymeric membrane separation to enrich H₂. This operating unit is also modelled with a SEP separator (MSEP1 in Fig. 2) in Aspen Plus wherein data are provided by previous studies (as demonstrated by Canete et al. [44], and the data are originally obtained from Ref. [50]). The enrichment of H₂ can also be achieved through different reforming techniques, such as a combination of DR and partial oxidation [51], or tri-reforming (TR) of DR, SR and partial oxidation [52]. However, partial oxidation often requires air separation units which may significantly increase the total capital cost of a plant. A fraction of the unreacted gas is purged to eliminate the accumulation of inert components. This effluent is flared producing CO₂ and water, but the heat it

Table 4

Reaction kinetic constants and parameters for the MeOH synthesis kinetic model. Data are obtained and rearranged from Ref. [47].

Reaction Constant	<i>E</i> _{ai} (J/mol)	<i>A</i> _i	<i>B</i> _i (K)
<i>k</i> ₁	-40,000	-29.87	4,811.16
<i>k</i> ₂	-	8.147	0
<i>k</i> ₃	-17,197	-6.452	2,068.44
<i>k</i> ₄	-124,119	-23.44	14,928.92
<i>k</i> ₅	98,084	4.804	-11,797.45
<i>k</i> ₆	18,705	17.55	-2,249.8
<i>k</i> ₇	58,393	0.131	-7,023.5

generates is not integrated due to technical and economic barriers [53].

The products from the RPLUG reactor (unit R2 in Fig. 2) flow through a series of flash tanks to separate the gaseous and liquid fractions. The first flash tank (FLTK2 in Fig. 2) separates most of the gaseous product at high pressure but low temperature in order to minimise re-compression work. The second flash tank (FLTK3 in Fig. 2) is operated at a reduced pressure for a better vapour-liquid separation. Although the liquid product from the second flash tank only contains trace amounts of light components, a third flash tank modelled with a SEP unit (FLTK4 in Fig. 2) is employed assuming perfect vapour-liquid separation, giving a liquid product composed of water and MeOH only. The low to trace amount of light components in the liquid product has an insignificant impact on the energy requirements of the distillation column, however a sharp separation is assumed for clarity. The distillation column is modelled with a RADFRAC unit giving a MeOH product at the top with a purity of 99.8 wt%. In the reference MeOH plant, the distillation column is optimised with a reflux ratio of 0.95 and 17 equilibrium stages in total. The raw product is fed at stage 10 of the column. Detailed fraction distribution at the corresponding stage is shown in Fig. 13 in Appendix A.

2.4. Electrification

The purpose of electrification is to substitute fossil fuel-based heating and feedstock with electricity. Our proposal for the electrification of MeOH production is presented in two ways. First, the reference process is electrified directly by implementing heat-pumps to reduce its heating requirement at an additional cost of mechanical work. Other direct electrification techniques based on electrothermal phenomena can be readily implemented in most chemical processes. However, heat-pumps are considered as a better option because they simultaneously reduce heating and cooling duties by upgrading the heat sources through mechanical compression and thus facilitate energy transhipment to the heat sinks. The efficiency of heat-pumps depends crucially on the temperature difference between heat source and sink. A graphical method based on the Grand Composite Curve (GCC) analysis is employed to determine the savings of hot and cold utilities as well as the required power for additional mechanical work.

The production of MeOH can also be electrified in an indirect way when alternative feedstocks are taken into account within electrification. Concretely, H₂ from water electrolysis is considered for the MeOH synthesis via CO₂ hydrogenation. This alternative path essentially substitutes the thermal energy of natural gas by the electricity that is consumed in H₂ production. The process flowsheet, adjusted to suit the change of feedstock, is shown in Fig. 3. The same reaction model is employed in the simulation of the MeOH synthesis via CO₂ hydrogenation. The change of feedstock from syngas (H₂ and CO) to CO₂ and H₂ (streams 1 and 3 in Fig. 3) inherits the same kinetics; however the exothermic reaction heat is less due to the lower energy content of the feed. In addition, the concentration of MeOH at the reactor outlet is much lower than that of a conventional plant based on natural gas reforming, resulting in a higher energy intensity at the downstream distillation. Indeed, the number of stages in the distillation column (DT1 in Fig. 3) is optimised to be 27 (larger than for the reference process) due to the lower MeOH concentration in the crude product (stream 26 in Fig. 3).

After plant-wide integration, the CO₂ hydrogenation plant can also be electrified directly by implementing a heat-pump, leading to a combined direct and indirect electrification case. The impact of both strategies are evaluated through sensitivity tests; all the scenarios are analysed in the following section based on environmental and economic assessments.

2.5. Environmental assessment

The environmental metrics take into account the process and indirect CO₂ emissions caused by energy utilisation (i.e. CO₂ generated due to heating or electricity consumption). The CO₂ emissions with respect to different energy sources are tabulated in Table 8 in Appendix

A; it is assumed that the marginal CO₂ emission from RES is zero. The net CO₂ balance is calculated by

$$net\text{CO}_2 = consumed\text{CO}_2 - (outlet\text{CO}_2 + indirect\text{CO}_2) \quad (23)$$

where *netCO₂* is the net abatement of CO₂ (kg), *consumedCO₂* is the mass (kg) of feedstock CO₂ that has been consumed in the process, *outletCO₂* represents the mass (kg) of emitted CO₂ from the process and *indirectCO₂* is the emission resulting from energy consumption. Notice that the unreacted components and waste MeOH in the purge stream are combusted to CO₂ and water before purging to the environment and thus they are included in the *outletCO₂* term. The energy (η_e) and carbon (η_c) efficiency are also selected as environmental indicators and calculated by

$$\eta_e = \frac{HHV_{MeOH}}{HHV_{NG} + Utilities} \times 100\% \quad (24)$$

$$\eta_c = \frac{Carbon\ in\ MeOH}{Carbon\ in\ feedstock} \times 100\% \quad (25)$$

where HHV_{MeOH} and HHV_{NG} indicate the high heating values of the MeOH product and natural gas feedstock, respectively. Notice that in the assessment the *Utilities* term excludes cooling duties.

2.6. Financial assessment

The financial performance of individual scenarios is evaluated based on two economic indicators, namely net present value (NPV) and internal rate of return (IRR). The value of NPV is calculated by

$$NPV = \sum_{t=1}^{20} \frac{C_t}{(1+r)^t} \quad (26)$$

where *C_t* is the cash flow of year *t* and *r* is the discount rate. The hurdle rate (the minimum expected return rate of a project) is assumed to be 8% in the analysis. The value of IRR indicates the discount rate *r* at which the NPV is zero. The annual *C_t* is determined by the difference between product revenue and operational expenditures (OpEx). The depreciation of the capital investment is also taken into account in the OpEx by assuming a linear depreciation over a course of 20 years with a salvage value of 5% total fixed capital cost (TFCC) after decommissioning. The value of TFCC is estimated by ratio factors based on the equipment cost of the main units as per the works of the Zhang et al. [54,55]. The calculation is shown in Eq. (27).

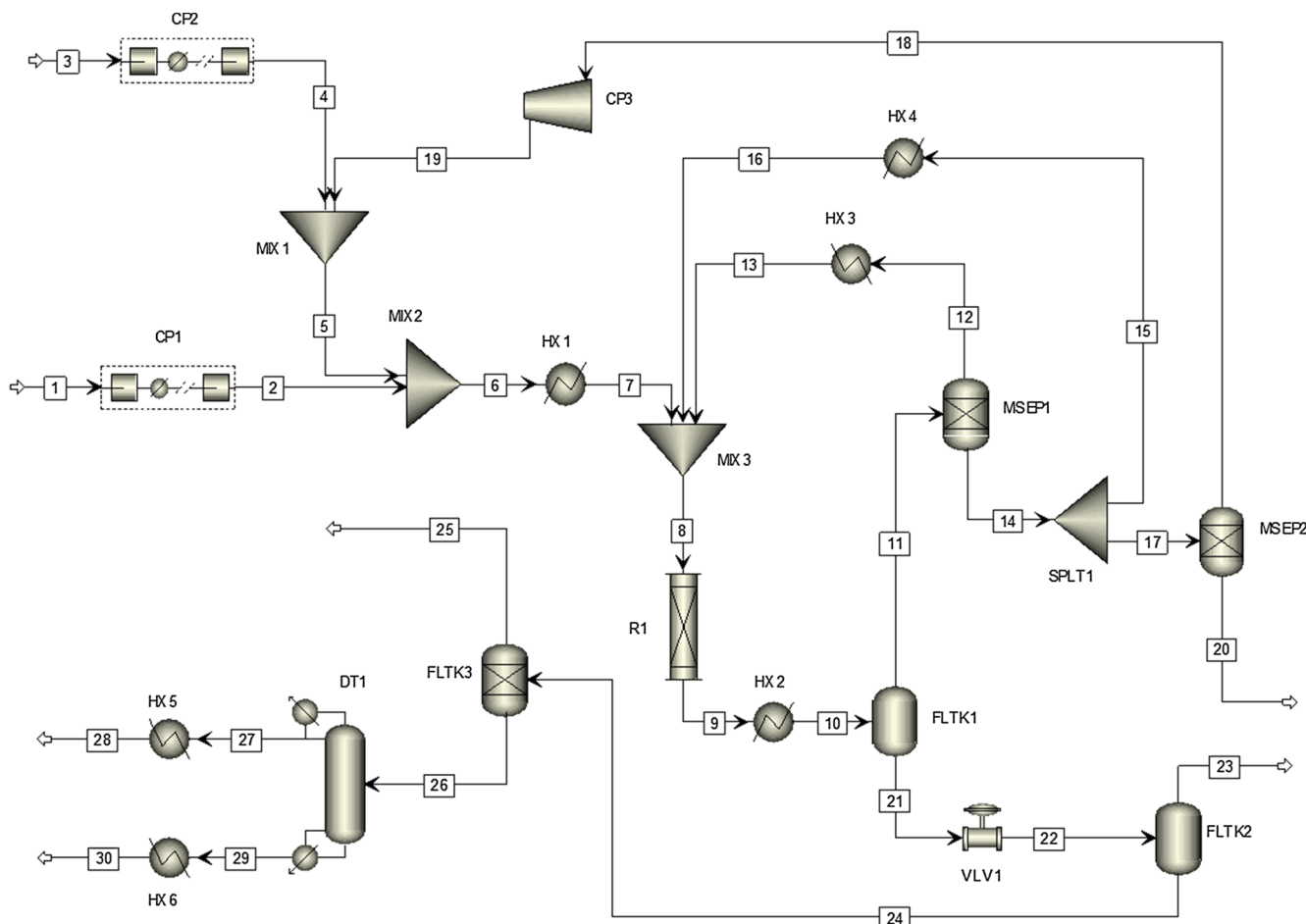
$$TFCC = Main\ units\ cost \times (1 + \sum \text{Ratio factor}) \quad (27)$$

Most equipment costs are directly reported after the simulation by Aspen Process Economic Analyser (APEA) based on the chemical engineering plant cost index (CEPCI) of 2018, whereas catalytic reactors (reformer and MeOH reactors) are estimated via the six-tenths factor rule based on literature values [56] and then updated to 2018 using the annual CEPCI. Since the CO₂ capture processes associated to each MeOH plant are not simulated up to scale (for simplicity, see assumptions in Section 2.7), their equipment costs are also determined via the six-tenths factor rule.

The calculation of OpEx considers utilities and raw materials costs, which are listed in Tables 9 and 10, respectively (see Appendix A). The cost ratios used to estimate utilities costs in Table 9 are obtained from Aspen Energy Analyzer. Taking electricity price as a basis (estimated to be 53.55 €/MWh [55]), the remaining utility costs are determined according to the cost ratio. The product prices are also summarised in Table 10 in Appendix A.

2.7. Assumptions used in the process design and analysis

The following assumptions have been used in this work: (1) the operation time of the processes is 8000 h per annum. (2) All the CO₂ feedstock is obtained via carbon capture from a flue gas source with conditions



UNIT

SPLT1 = splitter

MIX*i* = *i* th mixer

HX*i* = *i* th heat exchanger/cooler/heater

CP*i* = *i* th compressor/pump

FLTK*i* = *i* th flash tank

MSEP*i* = *i* th membrane separator

R1 = MeOH synthesis reactor

DT1 = distillation column

VVL1 = valve

Fig. 3. Process flow diagram of the non-conventional MeOH production plant simulated in Aspen Plus.

specified in Table 3. Although carbon capture from the MeOH production effluent consumes less energy (due to a higher CO₂ concentration), its additional capital cost may outweigh the saving from energy consumption. Since CO₂ capture is an auxiliary process, economic optimisation of the carbon capture unit is out of the scope of this work. (3) Energy from process flare is excluded from heat integration. (4) Multiple heat-pump implementation is not considered because its complexity (and thus its cost) significantly outweighs the potential benefit. (5) The compressors modelled in process simulation are assumed to be isentropic with an efficiency of 75%. (6) All mechanical work for both process and heat-pump compression is powered by electricity only. (7) The TFCC calculation only considers main equipment cost (excluding heat-pumps and other auxiliary units). (8) The price of electricity in the financial analysis is considered as an exogenous factor. However it is assumed to be 18 €/MWh in the base scenario of the sensitivity test. (9) Both environmental and financial assessments do not consider infrastructure construction and its potential impact.

3. Results and discussion

Several scenarios are considered in the analysis and then reported with their energy profiles. In the base case scenario (S1), a reference MeOH

plant based on conventional natural gas reforming is analysed and its utility consumption after energy integration is reported. This scenario represents most existing MeOH plants and its utility consumption is representative of current energy requirements. Scenario 2 (S2) reports utilities after direct electrification by implementing a heat-pump, which aims to explore the potential of electrification for the conventional MeOH plants using best available (and efficient) technology. The integrated CO₂ hydrogenation plant (S3) is regarded as an indirectly electrified process as its H₂ feedstock is obtained through electrolysis. This scenario represents a different strategy in the electrification of chemical processes but it requires a redesign of the flowsheet. Scenarios S4 – S6 consider combined direct and indirect electrification based on a CO₂ hydrogenation plant at an incremental level (increased energy transhipment). An overview of the analysis, integration boundaries and the resulting scenarios is illustrated in Fig. 4.

3.1. Materials and energy balance

The conceptual designs simulate a medium size MeOH production facility producing approximately 400,000 tonne per annum at an industry grade purity of 99.8 wt%. In the base case scenario the process consumes ca. 170,000 tonne of natural gas and 200,000 tonne of

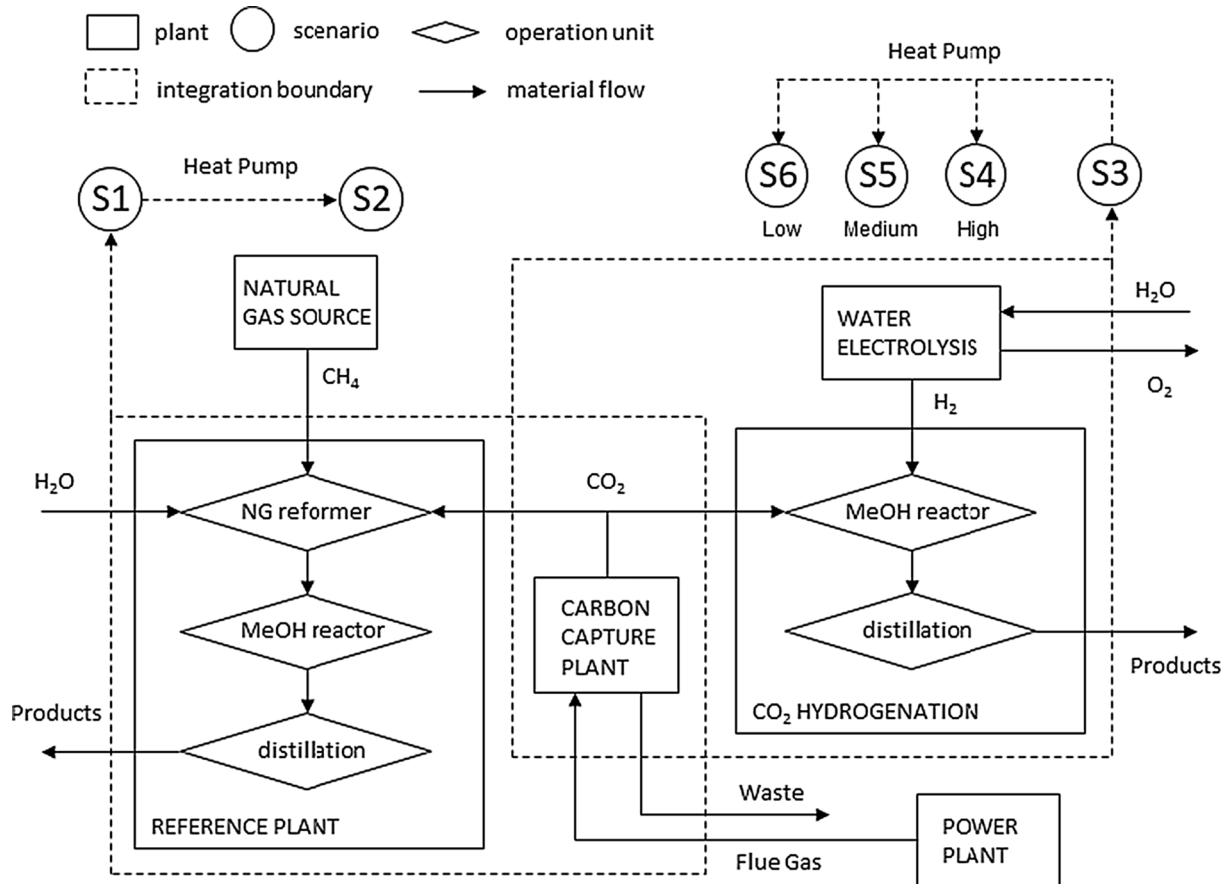


Fig. 4. Block representation of the scenarios and the analysis boundaries.

captured CO₂ per annum. The process also consumes approximately 157,000 tonne of water per year. The purge and effluent streams are flared thus producing CO₂ and water, for this reason the heat from these exothermic reactions (combustion) is not recovered. The overall purge rate is approximately 2% of the total production, which is consistent with conceptual designs from other sources [11,22]. It is possible to further reduce the amount of valuable product in the purge by adjusting flash tank conditions and thus increasing the capital cost of the recycling units. However, the optimisation of capital cost and product waste is beyond the scope of this work, and thus a typical operating condition is assumed.

In the reference process, the reformer (R1 in Fig. 2) is the major energy consumer powered by fossil fuel combustion at high temperature. The process is in heat surplus, however the major heat generator (R2 in Fig. 2) and its outlet stream can only provide low-grade heating; external heating is therefore required to meet the outstanding high-grade heating. After plant-wide integration, this process becomes scenario S1 in the analysis. The electrified reference process after heat-pump implementation has the same material balance but fewer hot and cold utilities (scenario S2). The detailed energy utilities with respect to the individual units in the reference plant are shown in Table 11 in Appendix A.

To produce the same amount of MeOH, the indirectly electrified process via CO₂ hydrogenation consumes approximately 78,000 tonne of H₂ and 650,000 tonne of captured CO₂ as feedstock per annum. The CO₂ feedstock is more than three times of that required in the reference MeOH plant but no fossil fuel feedstock is needed. The total energy consumption of the CO₂ hydrogenation plant is much higher when water electrolysis is taken into account. The loss of MeOH product due to the flashing process accounts for ca. 2% of the total production rate, which is consistent with the reference plant. The energy utilities of

individual units in the CO₂ hydrogenation plant are summarised in Table 12 in Appendix A. The integrated CO₂ hydrogenation plant is used for the sensitivity analysis as scenario S3, while scenarios S4 – S6 represent the same plant but implemented with a heat-pump at incremental levels.

The carbon capture process is designed to provide CO₂ feed to both the reference MeOH plant and the CO₂ hydrogenation plant. The energy utilities of individual units, summarised in Tables 13 and 14 in Appendix A, are scaled up in accordance with the requirement of the respective process they feed. Notice that the cooling utility of the desorber (DES in Fig. 1) is composed of two parts: (1) cooling water is used to cool the process stream to 40 °C; and (2) refrigeration is used to further cool it down to 18 °C. A makeup stream of MEA of 25.1 kg/h and 82.1 kg/h for the respective plant is used to compensate for the material lost to the ambient.

3.2. Energy integration and heat-pump implementation

The integration of energy utilities is analysed using the Aspen Energy Analyzer software. The heat cascade flow and GCC diagrams for each of the MeOH plants are plotted. Following a graphical analysis of the GCC diagrams, heat-pumps are implemented resulting in reduced theoretical hot and cold utilities at a cost of additional mechanical work. Such implementation provides an efficient way of increasing heat quality and thus facilitating the design of a heat-exchange network. However, the challenge often lies in the proper placement of the heat-pumps. In the seminal work of Townsend and Linnhoff, it is concluded that the heat-pumps should be implemented across the pinch in order to reduce energy utilities [57,58].

Fig. 5 illustrates the GCCs and their corresponding cascade diagrams for selected scenarios (GCCs for scenarios S4 and S5 are omitted).

Scenarios S1 and S3 represent the reference and the CO₂ hydrogenation plant respectively, and based on the resulting GCCs, direct electrification (S1 to S2, S3 to S4 – S6) can be implemented. The original GCCs before heat-pump implementation (blue curves in Fig. 5(A) and (B)) indicate the theoretical minimum heating (\dot{Q}_h) and cooling (\dot{Q}_c) utilities, and their values are shown in the cascade diagrams of Fig. 5. The shape of the respective GCCs are determined by the individual operating unit and its energy consumption characteristics. For instance, the top section of the GCC for S1 in Fig. 5(A) extends to a large enthalpy value at constant temperature due to the reformer operating at 950 °C, which is too high a temperature to be integrated. Since all scenarios contain heating or cooling requirements at virtually constant temperature, there are sections on the GCC that show nearly zero gradient, indicating infinite aggregated heat capacity (FC_p) of a process stream. To circumvent this computational difficulty, a temperature change of 0.1 °C is assumed for heating or cooling when the temperature is

constant. This characteristic of the process streams also results in large overlapping areas of the original and revised GCC (after heat-pump implementation). For clarity, the revised GCC of scenarios S4 and S5 are not shown.

As an example of the graphical analysis, the implementation of a heat-pump in S3 (resulting in S6) is shown in Fig. 5(B). Concretely, an amount of heat per unit time (\dot{Q}_2) is extracted from interval 15 at a temperature T_2 and transferred to interval 9 at T_1 . Notice that \dot{Q}_2 is marginally smaller than the enthalpy rate at the extraction temperature of T_2 (\dot{Q}_{T2}). This is because when \dot{Q}_2 is larger than \dot{Q}_{T2} , it results in a new pinch below T_2 and thus in a violation of the cross-pinchoff rule. When \dot{Q}_2 is equal to \dot{Q}_{T2} , it results in a double pinch GCC at T_2 and at the original pinch temperature. The heating utility saving, $\Delta\dot{Q}_H$, is equivalent to \dot{Q}_1 while the cooling utility saving $\Delta\dot{Q}_C$ is given by \dot{Q}_2 . Therefore, the revised GCC is shifted to the left horizontally by $\Delta\dot{Q}_H$ above the pinch and by $\Delta\dot{Q}_C$ below the pinch. In the intervals between T_1 and T_2 (exclusive), the GCC is unchanged, and thus the revised GCC superimposes the original sections.

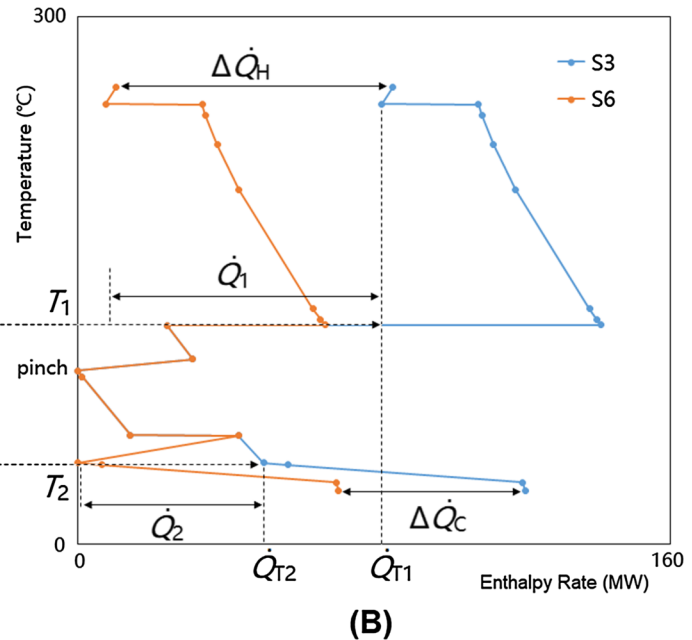
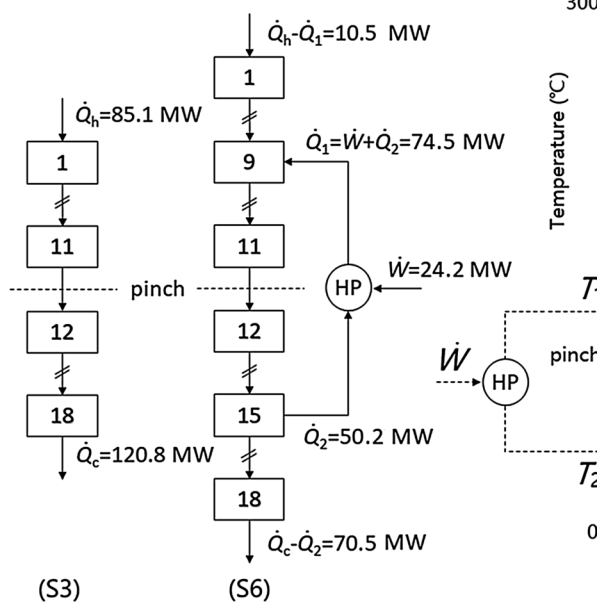
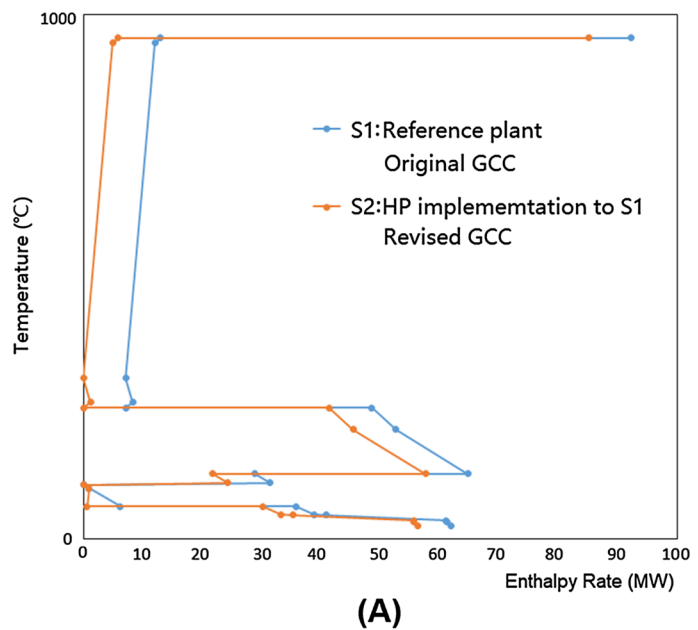
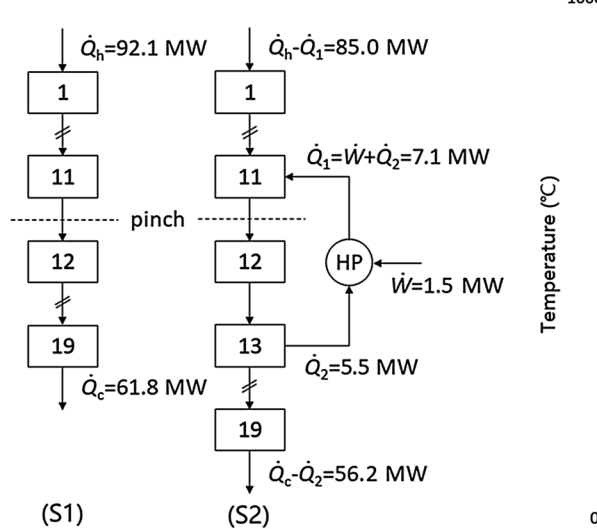


Fig. 5. Cascade diagrams and their corresponding Grand Composite Curves for (A) reference MeOH plant (S1) and its derived scenario (S2); (B) CO₂ hydrogenation MeOH plant (S3) and its derived scenario (S6).

The COP of the heat-pump is determined by

$$\text{COP} = \frac{\dot{Q}_1}{\dot{W}} = \frac{T^H}{T^H - T^L} \quad (28)$$

where T^H and T^L are the hot and cold temperatures (in Kelvin) of the working fluid, respectively. Notice that the temperature axis of the GCC diagrams is plotted using the average value of the hot and cold sides. When above the pinch, the working fluid acts as a hot stream and its temperature T^H coincides with the registered temperature on the hot side, i.e., $T^H = T_1 + 0.5\Delta T_{min}$, where ΔT_{min} is the temperature driving force, assumed to be 10 °C for both heat integration and heat-pump operation. On the other hand, T^L coincides with the registered temperature on the cold side since heat is extracted from the cold side to the working fluid, thus $T^L = (T_2 - 0.5\Delta T_{min}) - \Delta T_{min}$, where $(T_2 - 0.5\Delta T_{min})$ denotes the registered temperature on the cold side. Since the rate of mechanical work (\dot{W}) is equal to the difference between \dot{Q}_1 and \dot{Q}_2 , the COP equation can be rearranged into

$$\dot{Q}_2 = \frac{\dot{Q}_1(\text{COP} - 1)}{\text{COP}} \quad (29)$$

Therefore, either \dot{Q}_1 or \dot{Q}_2 is required to determine the other. The guideline is to choose the largest \dot{Q}_1 or \dot{Q}_2 while complying with the cross-pinches rules, i.e. satisfying the constraints that $\dot{Q}_1 \leq \dot{Q}_{T_1}$ and $\dot{Q}_2 \leq \dot{Q}_{T_2}$, simultaneously. As demonstrated in Fig. 5(B), \dot{Q}_{T_2} is the limiting factor determining the maximum effective heat transhipment whereas \dot{Q}_{T_1} is the limiting factor in Fig. 5(A) (not shown). The detailed utility savings and performance indicators of different scenarios are summarised in Table 5. Note that in the calculation an effective COP (COP_{eff}) is employed assuming 75% of Rankine cycle efficiency.

Although a heat-pump can be theoretically placed at a wide range of temperatures, in most practical cases its temperature lift is limited to ensure a satisfactory COP [59]. The exact location of temperature interval for heat-pump implementation is typically optimised through linear or non-linear programming (NLP) based on an objective function of utility cost [60,61], which is out of the scope of this work. Besides, the consideration of RES complicates the objective function of a traditional NLP. In the demonstrated examples, the placement of the heat-pump is decided using a heuristic method. For instance, in Fig. 5(A), the delivery temperature (T_1) is determined to be 109 °C because any hot utility saving greater than \dot{Q}_1 requires a much higher temperature lift (> 300 °C). As for the cold side, since \dot{Q}_1 is the limiting factor to satisfy the constraint, the optimal \dot{Q}_2 and its corresponding temperature can be estimated accordingly. Regarding S3 and its derived scenarios, heat-pumps are placed at an incremental level yet within reasonable temperature intervals (satisfactory COP). Another simplification for the work is that only a single heat-pump is considered for energy transhipment, and constraints are introduced to comply with the cross-pinches rule. However, in case of multiple heat-pumps implementation, these constraints are not necessarily true for an effective heat transfer. As first introduced by Rodera and Bagajewicz [62], heat transfer above or below the pinch by one heat-pump may act as “assisting” heat that can facilitate heat transfer when another heat-pump is implemented.

The electricity demands for heat-pump work and other operation

units are consolidated and illustrated in Fig. 6 along with other utility consumptions for the two MeOH plants and their derived scenarios. The heating utility is further stratified into low pressure (LP), medium pressure (MP), high pressure (HP), very high pressure (VHP) steam and fired heat (note HP steam consumption is null in all scenarios).

As depicted in Fig. 6, scenarios S1 and S2 have very similar energy structures because the direct electrification for the base case scenario (S1) can only substitute 7.8% of its total heating at an additional electricity consumption of 1.6 MW, both values are insignificant. The barrier preventing direct electrification is the large amount of high-grade heating (fired heat, accounting for 91.5% of the total heating in S1) required in natural gas reforming, which is difficult to substitute with electricity. Regarding the indirect electrification of S1 (S1 vs. S3), a significant increase in electricity demand (from 14.2 MW in S1 to 579.8 MW in S3) can

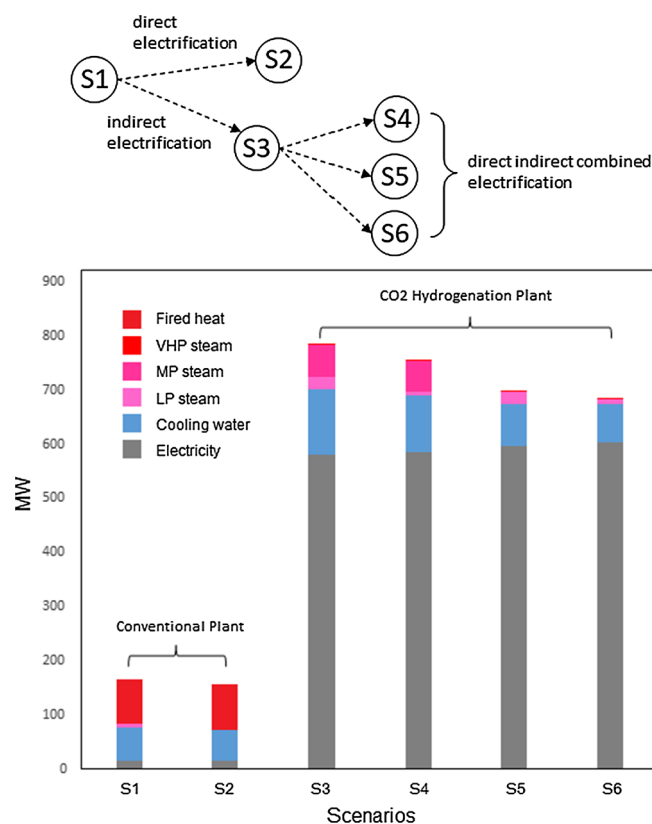


Fig. 6. Energy structure and consumption of different scenarios. (S1) Base scenario with conventional MeOH plant; (S2) direct electrification of S1 by heat-pump implementation; (S3) indirect electrification of S1 using H₂ produced from electrolysis; (S4) combined direct and indirect electrification with low heat-pump power; (S5) combined direct and indirect electrification with medium heat-pump power; (S6) combined direct and indirect electrification with high heat-pump power.

Table 5

Utility savings and performance indicators for different scenarios. Utility savings of S2 is derived taking S1 as a benchmark; utility savings of S4 – S6 are derived taking S3 as a benchmark.

Scenario Description	Utility Saving (MW)		HP Power (MW)	T^L (K)	T^H (K)	COP_{eff}	
	Hot	Cold					
S1	Base scenario of the reference plant	–	–	–	–	–	
S2	Direct electrification by HP implementation	7.12	5.57	1.70	320	382	4.61
S3	Indirect electrification using H ₂ as feedstock	–	–	–	–	–	–
S4	Combined electrification at low level	18.55	14.28	4.27	320	387	4.34
S5	Combined electrification at medium level	59.81	43.43	16.38	320	403	3.65
S6	Combined electrification at high level	74.54	50.27	24.27	304	403	3.07

be observed, which is attributed to the H₂ production in the CO₂ hydrogenation plant (accounting for 94% of the total electricity consumption in S3). Another noticeable difference between S1 and S3 is the heating requirement: although the reduction is insignificant (reduced from 92.1 MW in S1 to 85.1 MW in S3), the fired heat requirement is completely eliminated in S3 leaving only low-grade heating demand. This change in heating utilities provides additional opportunities when combined indirect and direct electrification is considered. Significantly, scenarios S4 – S6 gradually reduce the use of heating from 66.6 MW in S4 to 25.3 MW in S5 and eventually to 10.6 MW in S6. The reduction in heating (and thus a trend in achieving an almost fully electrified process) is of special interest as it facilitates the implementation and management of RES in chemical production. Although the direct electrification (S1 vs. S2) is insignificant, it has the advantage of a straightforward implementation. On the contrary, the indirect electrification strategy requires a new flowsheet design and thus is not applicable to existing chemical plants.

The energy content of fossil fuels is not a product of human effort and thus it has no cost except extraction, refining and transport cost. In direct contrast, H₂ production has a significant cost (aside from its transport and distribution costs), since a large amount of electricity is required to compensate the low energy content of feedstock, i.e. the water fed to the electrolysis plant has minimum energy content, as opposed to the natural gas fed to the conventional MeOH plant. Therefore, from the energy balance the CO₂ hydrogenation plants (scenarios S3 – S6) consume significantly more total energy in comparison with the reference plants (scenarios S1 and S2); however, the economic potential of the CO₂ hydrogenation plant is not necessarily inferior to its counterpart since their feedstock is of different value. The economic value of water and flue gas, which are the major feeds to the CO₂ hydrogenation plant, are much lower than that of natural gas. Another important factor that has to be taken into consideration is the source for electricity generation. If the electricity used to substitute natural gas is generated from fossil fuel, the overall process may not be energy efficient. However, electricity can be produced from RES and thus may have a much lower price (close to zero if RES is in surplus) than fossil fuels. Most importantly, its implication on environment is crucial.

3.3. Environmental assessment

The CO₂ balance, energy consumption and efficiency indicators for difference scenarios are tabulated in Table 6. From the process CO₂ balance, both the reference and the CO₂ hydrogenation plant (and their derived scenarios) consume more CO₂ as a feedstock than the directly emitted CO₂ in their flue gas. However, it may not necessarily result in an overall CO₂ abatement when CO₂ emissions from indirect sources are taken into consideration, as indicated by Eq. (23). Regarding the efficiency indicators, although the CO₂ hydrogenation plants (scenarios S3 – S6) demonstrate slightly better carbon efficiency, the energy efficiency is much lower than their counterpart conventional plants. This is mainly ascribed to the limit in water electrolysis, which may become a barrier to energy transformation in the future. However, when RES is introduced, the energy efficiency of a particular process may not be as

important. As commented by Dennis et al., the term “efficiency” (a coined word for emissions efficiency) may become more important in the future [63]. It is also noteworthy that direct electrification via a heat-pump implementation improves the energy efficiency in all scenarios, and is particularly effective in the CO₂ hydrogenation plants. This is attributed to the change in heating utilities (fired heat is eliminated) that facilitates such an implementation.

Since the CO₂ emissions from the electricity generated via coal are much higher than from direct heating via natural gas, the use of RES in electrification becomes pivotal in achieving the environmental targets. As illustrated in Fig. 7, CO₂ abatement of the CO₂ hydrogenation plant (and its derived scenarios, S3 – S6, with direct/indirect combined electrification) is highly sensitive to renewable penetration, surpassing the conventional processes (scenarios S1 and S2) at a renewable penetration of ca. 85% and achieving CO₂ emission neutrality at ca. 88%. Note that negative numbers mean a net CO₂ emission instead of abatement. At 100% renewable penetration, the CO₂ hydrogenation plant with a heat-pump implemented at the highest level (scenario S6) can achieve a CO₂ abatement of up to 1.35 kg/kg_{MeOH}, demonstrating a great potential in meeting environmental targets as well as CO₂ utilisation.

It is also noteworthy that in the analysis renewable sources are not considered for thermal heating because (1) scenarios S1 and S2 require heating at extremely high temperature which is difficult to be met by renewable sources; and (2) thermal heating utility is far less than the electricity consumption in scenarios S3 – S6. Consequently, the sensitivity to the change of renewable penetration is directly (and only) correlated to the total electricity consumption in each scenario. For instance, scenarios S1 and S2 are fairly insensitive to the renewable penetration due to the low electricity content in their utilities. The direct electrification by heat-pump implementation in CO₂ hydrogenation plants reduces the CO₂ abatement when renewable penetration is low; however an opposite trend is shown when the penetration is high (shown in the inset of Fig. 7). This is attributed to the fact that CO₂ abatement from hot utility savings overweighs the additional CO₂ contribution from the mechanical work of the heat-pump when renewable penetration is high.

3.4. Financial assessment

Before assessing the economic feasibility of each scenario, the equipment cost of the main units with respect to the reference plant and the CO₂ hydrogenation plant are estimated, as shown in Table 7. Most of the values are directly reported from simulation results except the catalytic reactors (reformer and MeOH reactor). The cost of the reactors

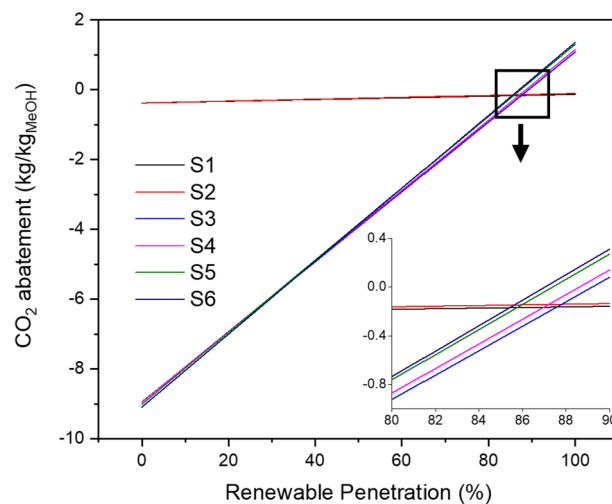


Fig. 7. Influence of renewable penetration on CO₂ abatement for different scenarios. The inset shows the enlarged section in the range of 80 – 90% of renewable penetration.

Table 6
Summary of key environmental indicators for each scenarios.

	S1	S2	S3	S4	S5	S6
Balance (kg/kg_{MeOH})						
consumedCO ₂	0.50	0.50	1.64	1.64	1.64	1.64
outletCO ₂	0.30	0.30	0.25	0.25	0.25	0.25
Utility (MW)						
Heating	92.1	85.0	85.1	66.6	25.3	10.6
Electricity	14.2	15.7	579.8	584.1	596.2	604.1
Efficiency (%)						
Energy	73.2	74.1	47.6	48.7	50.9	51.5
Carbon	82.0	82.0	83.6	83.6	83.6	83.6

Table 7
Main equipment cost estimation for each plant.

No.	Unit	Reference plant (M€)	CO ₂ hydrogenation plant (M€)	Source
1	Reformer	12.20	–	[56]
2	MeOH reactor	13.97	13.12	[56]
3	Syngas flash tank	0.03	–	APEA
4	Distillation column	0.58	0.73	APEA
5	MeOH flash tanks	0.18	0.25	APEA
6	Compressors	6.68	41.59	APEA
7	Coolers	0.31	0.49	APEA
8	Heaters	0.09	0.21	APEA
9	Absorber	13.94	28.38	APEA
10	Desorber	5.22	10.63	APEA

are scaled via the six-tenths factor rule based on literature values [56]. As demonstrated in Table 7, a noticeable difference in the respective plant is from the equipment cost of compressors, which is attributed to the change of feedstock in the CO₂ hydrogenation plant. The values of TFCC are estimated by ratio factors and detailed items are summarised in Table 15 in Appendix A. Notice that the TFCC of the heat-pump is ignored since its value is too small in comparison with the plant cost. However, the additional electricity consumption due to heat-pump implementation is considered in the OpEx.

Fig. 8 shows the NPV of all scenarios by varying the price of electricity. The current market price of electricity is around 50 €/MWh, however it is possible to find RES with a price lower than 20 €/MWh [64]. In the case of surplus RES, the generated electricity often has a very low price or is even close to free of charge. In the current market, the CO₂ hydrogenation plant and its derived scenarios (S3 – S6) all have a negative NPV, whereas the reference plant and its derived scenarios (S1 – S2) have an NPV above 800 M€. However, electricity from RES may have a lower price and thus facilitating the profitability of the electrified scenarios. It is estimated that the CO₂ hydrogenation plants achieve a positive NPV when electricity price is below 22 €/MWh, and its economic potential exceeds the reference MeOH plants when the electricity price is in the range of 3–4 €/MWh, depending on the extent of direct electrification (see the inset in Fig. 8). The NPV of CO₂ hydrogenation plants is also compared with a similar design (and size) process proposed by Perez-Fortes et al. [22]. In the current market, the NPV of CO₂ hydrogenation plants from our simulation is around –1200 M€, whereas Perez-Fortes et al. reported –1036.2 M€ in the base scenario [22]. The difference may be attributed to the alternative methods in CapEx and TFCC estimation.

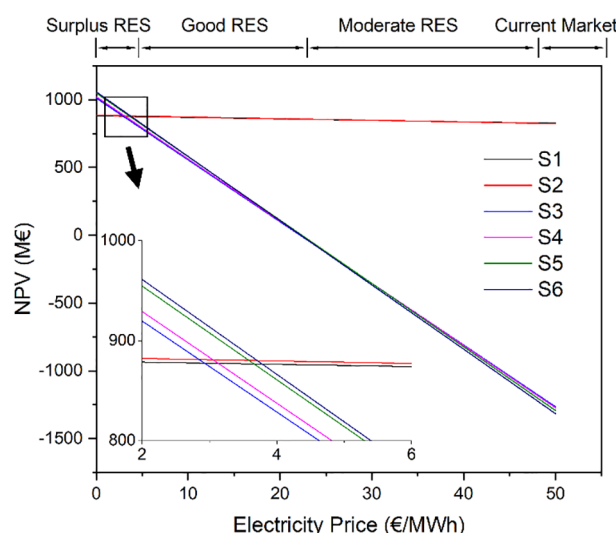


Fig. 8. NPV values of each scenario with varying electricity prices. The inset shows the enlarged section ranging from 2 to 6 €/MWh.

In analogy to the CO₂ emissions, the influence of heat-pump implementation on NPV switches at a specific electricity price. For instance, heat-pump reduces the NPV when the electricity price is higher than 30 €/MWh for the CO₂ hydrogenation plants, but its implementation improves the NPV when the price is below 20 €/MWh. From the thermodynamic principle of a heat-pump, the economic performance can be derived and is governed by

$$\text{COP}_{\min} = \frac{\text{Price}_{\text{electricity}} + \text{Price}_{\text{cooling}}}{\text{Price}_{\text{heating}} + \text{Price}_{\text{cooling}}} \quad (30)$$

where COP_{min} is the minimum coefficient of performance that would result in an economical implementation of a heat-pump. In the current energy market the COP_{min} is calculated to be 6.68, which is higher than the COP of the heat-pumps implemented in all scenarios (see Table 5). When RES is used (implying a lower electricity price), it eases the constraint on COP_{min} and thus improves the economic feasibility of direct electrification.

It is also worthy to note that the influence of a heat-pump is marginal when compared to the indirect electrification (S1 to S3). However, the significance of heat-pumps lies in their facile implementation. In contrast, indirect electrification requires re-design of the flowsheet to accommodate the change of feedstock, which is inapplicable to most existing plants.

3.5. Sensitivity analyses

The uncertainties in selected key variables (e.g., electricity price, MeOH price, TFCC, natural gas (NG) price and CO₂ price) are investigated through sensitivity analyses. Since the influence of indirect electrification significantly outweighs the direct electrification in the economic evaluation, the sensitivity analyses of S1 and S2 behave similarly (and the same can be said for S3 and its derived scenarios S4 – S6). In contrast, S1 and S3 (the latter representing indirect electrification) behave differently. The parameters for 0% variation (base case in sensitivity test) are tabulated in Table 16 in Appendix A.

As illustrated in Fig. 9, the IRR values for all scenarios are highly dependent on MeOH price. When MeOH price is increased from 400 to 600 €/tonne, the IRR values of scenarios S1 and S3 increase to 75.4% and 36.1%, respectively. Scenario S3 (and its derived scenarios S4 – S6) is more sensitive to the change of CO₂ price and electricity price than S1 and S2. This is attributed to the large quantity of CO₂ feedstock and electricity consumed in the CO₂ hydrogenation plants. The price of CO₂ means that the process receives a revenue for using captured CO₂ and a baseline price of 40 €/tonne is assumed in the analysis. The IRR value of the reference plant (S1) is least dependent on the change of NG price. Regarding the CO₂ hydrogenation plants (S3 – S6), their IRR is independent on natural gas since no fossil fuels are used in the process.

The influence of TFCC is also significant for all scenarios, highlighting the importance of economies of scale (since TFCC per unit mass of product reduces when the scale of production increases). The simulated processes have an annual production rate of 400,000 tonne, which is a medium size plant in the context of modern MeOH production. Thus, there is room to improve the economic performance when a larger scale is considered.

It is important to point out that the reference plant (S1) and its derived scenario (S2) have shown a satisfactory IRR in all circumstances within the range considered. The same cannot be said of the CO₂ hydrogenation plants (S3 – S6, note the hurdle rate is set to be 8%). Clearly, the economic potential of the conventional MeOH process is unimpeachable compared to the indirectly electrified process. Nevertheless, the significance of electrification lies mainly in the environmental impact. Moreover, in the case of surplus RES the electrified process has shown a better economic performance. The use of surplus RES to power MeOH production is of special interest because it is not only economically viable but also provides a solution to store renewable energy in the form of MeOH. This idea can be extended to the electrified

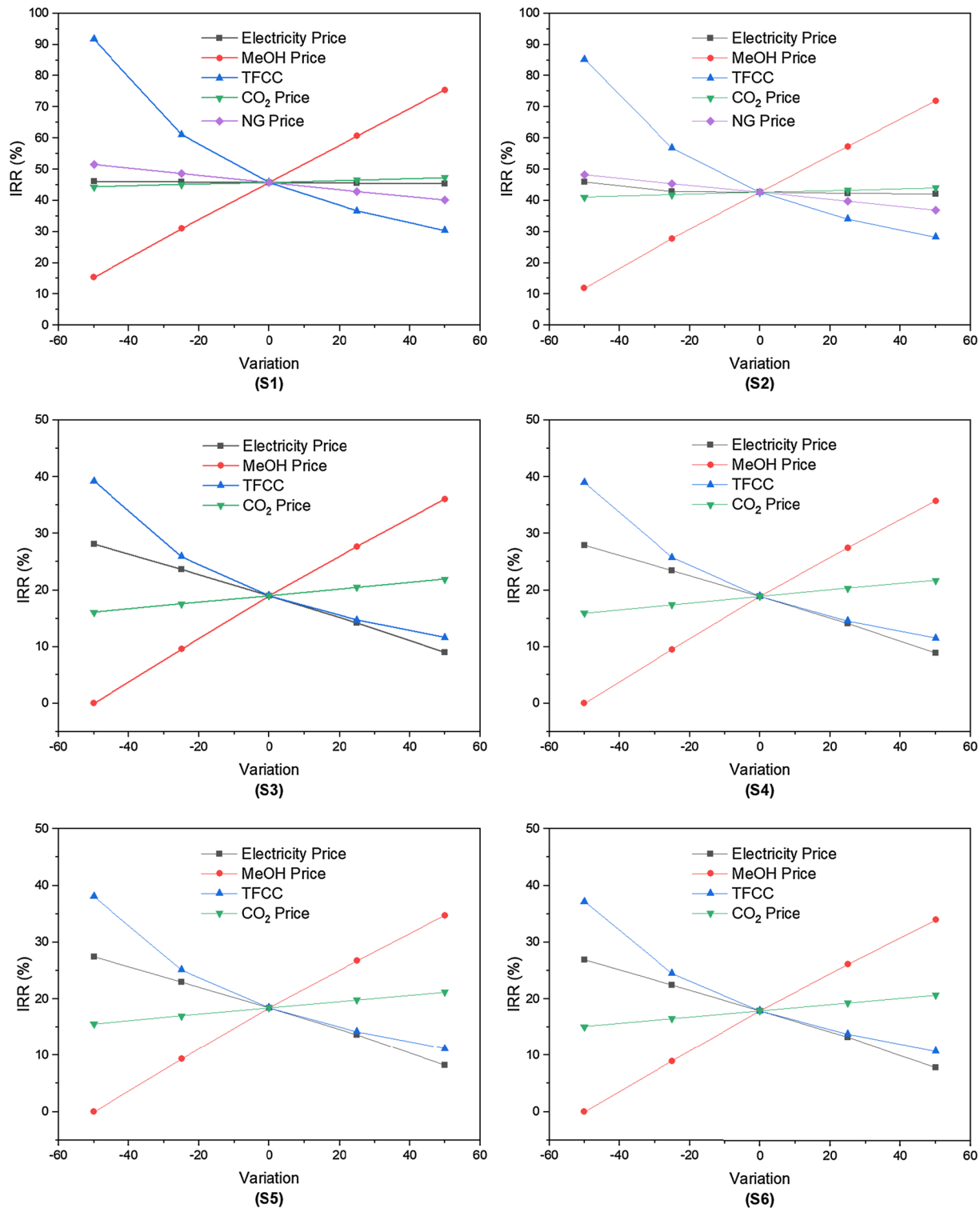


Fig. 9. Sensitivity analysis of all scenarios.

production of any other high heating value chemicals, and thus it opens up new ways of thinking about RES storage and management.

4. Future work

This work is the first of a series. As a next step, and based on the energy analysis of this work, RES will be introduced to power the fully electrified MeOH production process. In previous studies, Beerbuhl et al. reported a novel optimisation method to integrate RES in electricity-based NH₃

production [65]. Nayak-Luke et al. also investigated the impact of RES intermittency on plant sizing and economic performance [8]. However, most previous studies on RES integration have focused on NH₃ and integration to RES is still missing for MeOH production. This integration is significant not only because of its energy and market value, but also because of its process characteristics: the distillation of raw MeOH product, which is an important energy consumer in the process, provides an additional handle for RES management. Intermittency would be accounted for by storing raw MeOH as an intermediate product to match RES variability.

As a comparison, NH₃ production can mainly accommodate RES intermittency through demand side management, resulting in oversizing the electrolyzers (and thus increasing the process CapEx) [8]. The separation of the catalytic reaction (to produce raw MeOH) and distillation process (to produce refined MeOH) enhances the process flexibility to better suit the variability of RES. To this end, new design variables will be considered to address the combined scheduling (RES and dispatchable energy) and sizing (electrolyser, catalytic reactor and distillation column) of electricity-based MeOH production.

Other than producing MeOH as a commodity, energy storage system (ESS) can be designed with MeOH as an energy vector. Originally, Banares-Alcantara et al. proposed a conceptual design of a NH₃ based ESS for an islanded system [66], and Wang et al. recently analysed the time-invariant performance of such a concept [67]. With the developments in direct methanol fuel cell [68,69], the same concept can be applied to MeOH based ESS with advantages in long-term storage and facile transportation. Although the complexity in MeOH production poses a modelling difficulty, it offers additional design variables for optimisation. We envision that the design of MeOH based ESS, which is benefited by its unique process characteristics, may become a future solution to the utilisation of surplus RES.

5. Conclusions

The analysis in this work considers both direct and indirect electrification schemes in MeOH production. Indirect electrification using alternative feedstock has demonstrated a remarkable potential in both environmental and economic assessments. However, due to the feedstock change to low energy content materials (water and flue gas), the total energy consumption of a CO₂ hydrogenation plant (which is considered as an indirectly electrified plant) is inevitably and substantially larger than the traditional process. The low energy efficiency (mainly because of the water electrolysis units) of the CO₂ hydrogenation plant also contributes to the large energy demand. In addition, the economic performance of electrification crucially relies on renewable penetration as the cost of electricity generated from fossil fuels outweighs that of their use for heating per unit energy. In other words, it is viable to substitute the energy content in fossil fuels with electricity

only if inexpensive RES are used. The almost fully electrified process (S6) reaches a break-even point and improves on a conventional plant (S1) at an electricity price of 22 €/MWh and 4 €/MWh, respectively. Regarding the environmental impact, the best scenario of indirect/direct combined electrification can reach a CO₂ abatement of up to 1.35 kg/kg_{MeOH} at 100% renewable penetration.

Direct electrification through heat-pump implementation is insignificant when compared to indirect electrification. Its impact is limited by the heat that can be delivered by a heat-pump. As an example, the largest case of direct electrification (S3 to S6) can only convert 74.5 MW of heating (accounting for 87.5% of total heating in S3) at an additional cost of 24.3 MW of electricity (accounting for 4.0% of total electricity in S6). In contrast, indirect electrification (S1 to S3) increases the electricity consumption from 14.2 MW in S1 to 604.1 MW in S3, with 90.3% of the electricity (545.7 MW) consumed in feedstock (H₂) synthesis. The key implications for policymakers are clear: (1) modification of current industrial processes may have an insignificant impact on energy transition, and thus new process designs should be explored instead. (2) Energy policies should plan for a significant increase in power demand. From our analysis, the fully electrified MeOH production consumes 6 – 7 times more energy than the traditional fossil based process. (3) Renewable power deployment has to be accelerated in the near future and in tandem with the progress in electrification, ensuring that increased electricity demand will be met by zero-carbon resources. We hope this work can provide a technological and economic basis for future scenarios and facilitate the wholesale transition of fossil fuel to electricity in chemical industry.

6. Notes

The authors declare no conflict of interest.

Acknowledgements

The first two authors are grateful for the funds provided by the China Scholarship Council. The authors wish to thank Prof. Lei Xing for insightful discussions.

Appendix A

See Figs. 10–13.

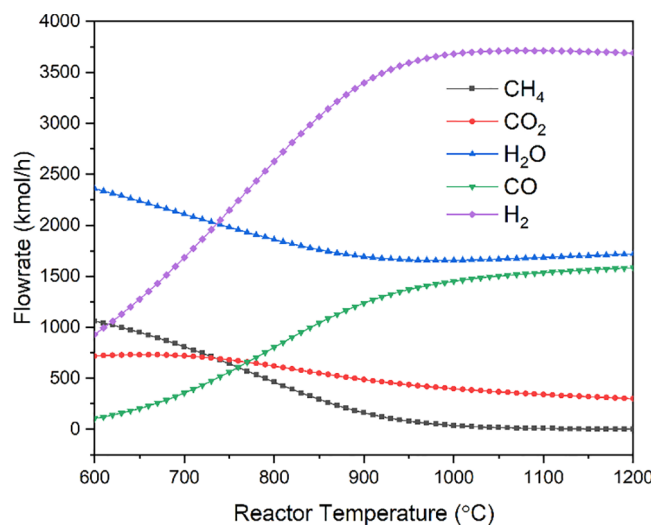


Fig. 10. Flowrates of all species in the produced sygas with respect to reactor temperature.

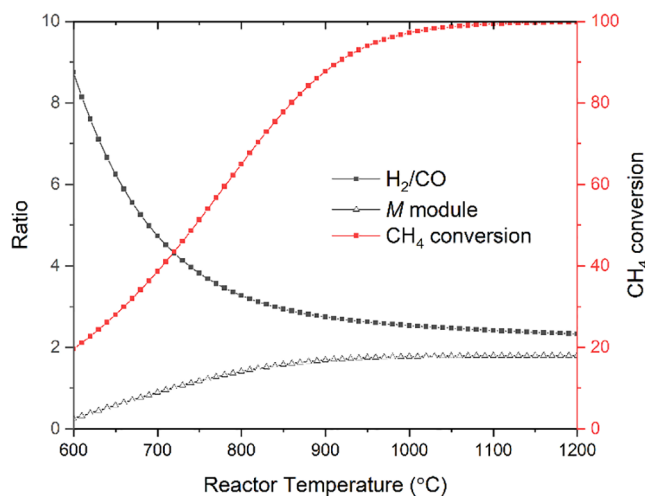


Fig. 11. Profiles of H₂/CO, M module and CH₄ conversion with respect to reactor temperature.

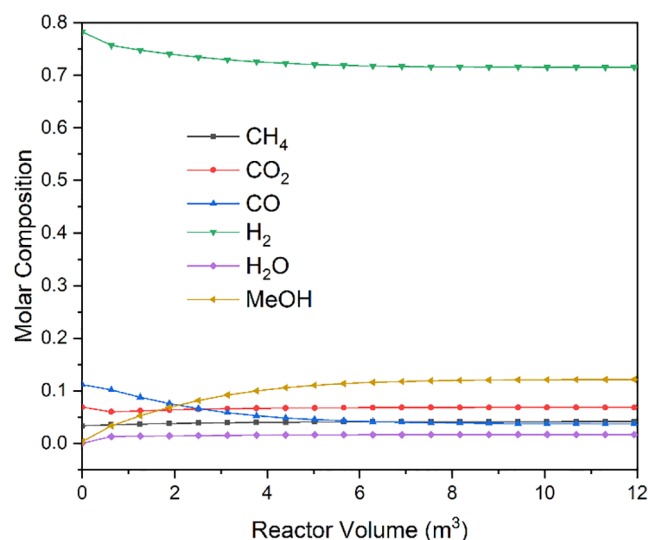


Fig. 12. Molar composition of species in the MeOH reactor.

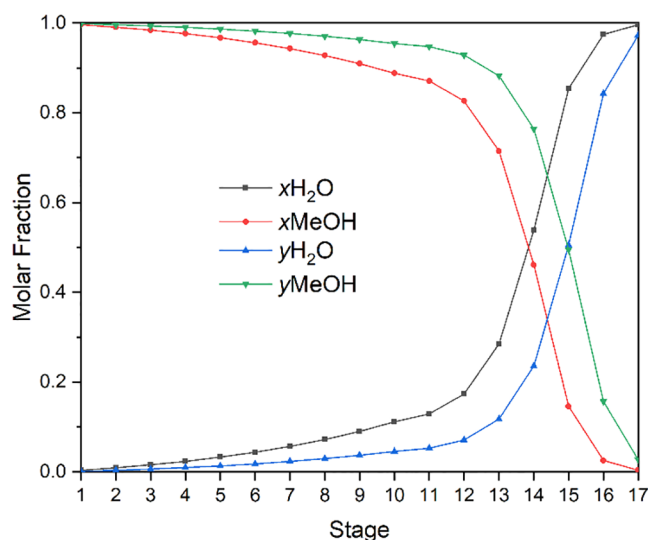


Fig. 13. Fraction distribution of MeOH and water in both liquid (x) and vapour (y) phase at the corresponding distillation stage (unit DT in Fig. 2). Sharp liquid-vapour separation upstream is assumed.

See Tables 8–16.

Table 8
CO₂ emission for different utilities. Data are obtained from Ref. [70].

Utility	Source	CO ₂ emission (kg/kWh)
Heating	Natural gas combustion	0.18
Electricity	Pulverised coal plant	0.86
Electricity	RES	0

Table 9
Price for utilities and their corresponding supply temperature.

Utility	Cost (€/MWh)	Supply Temperature (°C)
Cooling water	0.72	25
LP steam	6.48	125
MP steam	7.49	175
HP steam	8.50	250
VHP steam	11.88	400
Fired heat	14.40	1,000
Electricity	53.55	–

Table 10
Raw material and product price (all currency is converted to € based on 1 USD = 0.88 €).

	Price	Unit	Source
MeOH	400	€/tonne	[22]
Natural gas	3.48	€/MMBtu	[43]
Process water	0.02	€/tonne	[43]

Table 11

Summary of the utility use in the reference MeOH plant (Fig. 2) before heat integration.

No.	Unit Name	Inlet Stream		Outlet Stream		Duty (kW)	Utility
		P (bar)	T (°C)	P (bar)	T (°C)		
R1	Reformer	20.0	949.8	20.0	950.0	79,114.1	Fired heat
R2	MeOH Reactor	71.0	255.0	70.0	255.0	–41,333.4	Cooling water
HX1	Heater	20.0	301.5	20.0	950.0	21,466.4	Fired heat
HX2	Heater	19.5	28.0	20.0	950.0	58,800.4	Fired heat
HX3	Cooler	20.0	950.0	19.5	30.0	–82,072.6	Cooling water
HX4	Heater	71.0	203.3	71.0	255.0	2,443.7	VHP steam
HX5	Cooler	70.0	255.0	70.0	40.0	–46,535.2	Cooling water
HX6	Heater	70.0	40.0	71.0	255.0	19,837.2	VHP steam
HX7	Heater	70.0	40.0	71.0	255.0	1,050.7	VHP steam
HX8	Cooler	1.1	66.7	1.0	40.0	–1,181.1	Cooling water
HX9	Cooler	1.1	101.7	1.0	40.0	–287.3	Cooling water
DT1	Condenser	1.1	66.8	1.1	66.7	–29,571.1	Cooling water
DT1	Reboiler	1.1	98.2	1.1	101.7	31,906.8	LP steam
CP1	Compressor	2.0	40.0	20.0	282.0	3,772.1	Electricity
CP2	Compressor	1.0	30.0	20.0	350.3	2,157.7	Electricity
CP3	Pump	1.0	25.0	20.0	25.2	13.1	Electricity
CP4	Compressor	19.5	30.0	71.0	203.3	8,032.5	Electricity

Table 12Summary of the utility use in the CO₂ hydrogenation plant (Fig. 3) before heat integration.

No.	Unit Name	Inlet Stream		Outlet Stream		Duty (kW)	Utility
		P (bar)	T (°C)	P (bar)	T (°C)		
R1	MeOH Reactor	71.0	255.0	70.0	255.0	-26,011.9	Cooling water
HX1	Heater	71.0	196.2	71.0	255.0	3,990.1	VHP steam
HX2	Cooler	70.0	255.0	70.0	40.0	-94,737.8	Cooling water
HX3	Heater	70.0	40.0	71.0	255.0	4,349.4	VHP steam
HX4	Heater	70.0	40.0	71.0	255.0	43,824.7	VHP steam
HX5	Cooler	1.1	66.7	1.0	40.0	-1,209.5	Cooling water
HX6	Cooler	1.1	100.0	1.0	40.0	-2,143.2	Cooling water
DT1	Condenser	1.1	66.8	1.1	66.7	-29,110.7	Cooling water
DT1	Reboiler	1.1	93.5	1.1	100.0	33,423.3	LP steam
CP1	Cooler-1	3.1	132.7	3.1	35.0	-2,004.4	Cooling water
CP1	Cooler-2	8.8	138.7	8.8	35.0	-2,134.1	Cooling water
CP1	Cooler-3	25.0	138.7	25.0	35.0	-2,134.1	Cooling water
CP2	Cooler-1	4.1	232.1	4.1	35.0	-7,763.4	Cooling water
CP2	Cooler-2	17.1	248.8	17.1	35.0	-8,422.8	Cooling water
CP1	Multi-compressor	1.1	30.0	71.0	138.7	8,503.5	Electricity
CP2	Multi-compressor	1.0	25.0	71.0	248.8	24,997.8	Electricity
CP3	Compressor	70.0	40.0	71.0	41.7	8.9	Electricity

Table 13

Summary of the utility use in the carbon capture process (Fig. 1) with regards to the reference plant.

No.	Unit Name	Inlet Stream		Outlet Stream		Duty (kW)	Utility
		P (bar)	T (°C)	P (bar)	T (°C)		
HX1	Cooler	2.0	59.1	2.0	40.0	-19,185.8	Cooling water
DES	Condenser	2.0	108.8	2.0	40.0	-15,523.6	Cooling water
DES	Condenser	2.0	40.0	2.0	18.0	171.0	Electricity
DES	Reboiler	2.0	119.3	2.0	119.3	35,825.8	LP steam
COMP1	Pump	1.0	48.6	2.0	48.6	1.1	Electricity
COMP2	Pump	1.0	53.3	2.9	53.1	177.0	Electricity

Table 14Summary of the utility use in the carbon capture process (Fig. 1) with regards to the CO₂ hydrogenation plant.

No.	Unit Name	Inlet Stream		Outlet Stream		Duty (kW)	Utility
		P (bar)	T (°C)	P (bar)	T (°C)		
HX1	Cooler	2.0	59.1	2.0	40.0	-62,716.7	Cooling water
DES	Condenser	2.0	108.8	2.0	40.0	-50,745.2	Cooling water
DES	Condenser	2.0	40.0	2.0	18.0	558.9	Electricity
DES	Reboiler	2.0	119.3	2.0	119.3	117,111.3	LP steam
COMP1	Pump	1.0	48.6	2.0	48.6	3.5	Electricity
COMP2	Pump	1.0	53.3	2.9	53.1	578.5	Electricity

Table 15

Total fixed capital cost estimation for each plant.

Items	Ratio factor	Reference plant (M€)	CO ₂ hydrogenation plant (M€)
Purchased equipment cost	1.00	53.20	95.41
Installation cost	0.47	25.00	44.84
Instrumentation and controls	0.36	19.15	34.35
Piping	0.68	36.18	64.88
Electrical systems	0.11	5.85	10.49
Building and services	0.18	9.58	17.17
Yard improvements	0.10	5.32	9.54
Service facilities	0.70	37.24	66.78
<i>Total direct cost</i>		191.52	343.46
Engineering and supervision	0.33	17.56	31.48
Construction expenses	0.41	21.81	39.12
Legal expenses	0.04	2.13	3.82
Contractor's fee	0.22	11.70	20.99
Contingency	0.44	23.41	41.98
<i>Total indirect cost</i>		76.61	137.38
TFCC		268.1	480.8

Table 16
Parameters for 0% variance in the sensitivity test.

	Reference plant	CO ₂ hydrogenation plant	Unit
Electricity	18	18	€/MWh
MeOH price	400	400	€/tonne
TFCC	268	481	M€
Natural gas price	182	—	€/tonne
OpEx excluding natural gas	5.9	86.4	M€/year
CO ₂ price	40	40	€/tonne

References

- [1] Reaching net-zero carbon emissions from harder-to-abate sectors by mid-century. Report. Energy Transitions Commission. 2018.
- [2] Kafandaris S. Buying greenhouse insurance: the economic costs of CO₂ emission limits. *J Operation Res Soc* 1994;45:479–80.
- [3] Tangeras TP. Renewable electricity policy and market integration. *Energy J* 2015;36:331–53.
- [4] Sugiyama M. Climate change mitigation and electrification. *Energy Policy* 2012;44:464–8.
- [5] Searchinger T, Heimlich R, Houghton RA, Dong FX, Elobeid A, Fabiosa J, et al. Use of US croplands for biofuels increases greenhouse gases through emissions from land-use change. *Science* 2008;319:1238–40.
- [6] Logan BE, Rabaey K. Conversion of wastes into bioelectricity and chemicals by using microbial electrochemical technologies. *Science* 2012;337:686–90.
- [7] Kranenburg Kv, Schols E, Gelevert H, Kler Rd, Delft Yv, Weeda M. Empowering the Chemical Industry: Opportunities for Electrification. Report. TNO; 2016.
- [8] Nayak-Luke R, Bañares-Alcántara R, Wilkinson I. “Green” ammonia: impact of renewable energy intermittency on plant sizing and leveled cost of ammonia. *Ind Eng Chem Res* 2018;57:14607–16.
- [9] Peng S-Y, Jin G-P, Cui J-S, Lv X-Y, Yu Y-X, Tang H-W. Preparation of nickel hexacyanoferrate/heterogeneous carbon composites for CO₂ continuous electrocatalytic reduction to formic acid. *J Environ Chem Eng* 2018;6:6931–8.
- [10] Zhao Z, Fan J, Xie M, Wang Z. Photo-catalytic reduction of carbon dioxide with in-situ synthesized CoPc/TiO₂ under visible light irradiation. *J Cleaner Prod* 2009;17:1025–9.
- [11] Van-Dal ES, Bouallou C. Design and simulation of a methanol production plant from CO₂ hydrogenation. *J Cleaner Prod* 2013;57:38–45.
- [12] Deng L, Adams TA. Methanol production from coke oven gas and blast furnace gas. *Comp Aided Chem Eng* 2018;44:163–8.
- [13] Bukhtiyarova M, Lunkenbein T, Kähler K, Schlägl R. Methanol synthesis from industrial CO₂ sources: a contribution to chemical energy conversion. *Catal Lett* 2017;147:416–27.
- [14] Alsagheh S, Johnson JR, Ohs B, Wessling M. Methanol production via direct carbon dioxide hydrogenation using hydrogen from photocatalytic water splitting: Process development and techno-economic analysis. *J Cleaner Prod* 2019;208:1446–58.
- [15] Arakawa H. Research and development on new synthetic routes for basic chemicals by catalytic hydrogenation of CO₂. In: Inui T, Anpo M, Izui K, Yanagida S, Yamaguchi T, editors. Studies in Surface Science and Catalysis. Elsevier; 1998. p. 19–30.
- [16] Aresta M, Dibenedetto A. Utilisation of CO₂ as a chemical feedstock: opportunities and challenges. *Dalton Trans* 2007;2975–2992.
- [17] Harnisch F, Ross LFM, Kracke F, Virdis B, Krömer JO. Electrifying white biotechnology: engineering and economic potential of electricity-driven bio-production. *ChemSusChem* 2015;8:758–66.
- [18] Nayak-Luke RM, Bañares-Alcántara R. Long-term energy storage: what is the need and is ammonia a solution? *Comp Aided Chem Eng* 2018;44:1843–8.
- [19] Ebrahimi S, Mac Kinnon M, Brouwer J. California end-use electrification impacts on carbon neutrality and clean air. *Appl Energy* 2018;213:435–49.
- [20] Lechtenböhmer S, Nilsson LJ, Åhman M, Schneider C. Decarbonising the energy intensive basic materials industry through electrification – implications for future EU electricity demand. *Energy* 2016;115:1623–31.
- [21] Charoensuppanimit P, Kitsahawong K, Kim-Lohsoontorn P, Assabumrungrat S. Incorporation of hydrogen by-product from NaOCH₃ production for methanol synthesis via CO₂ hydrogenation: Process analysis and economic evaluation. *J Cleaner Prod* 2019;212:893–909.
- [22] Perez-Fortes M, Schoneberger JC, Boulamant A, Tzimas E. Methanol synthesis using captured CO₂ as raw material: Techno-economic and environmental assessment. *Appl Energy* 2016;161:718–32.
- [23] Ren SJ, Shoemaker WR, Wang XF, Shang ZY, Klinghoffer N, Li SG, et al. Highly active and selective Cu-ZnO based catalyst for methanol and dimethyl ether synthesis via CO₂ hydrogenation. *Fuel* 2019;239:1125–33.
- [24] Chen JY, Wang X, Wu DK, Zhang JL, Ma QX, Gao XH, et al. Hydrogenation of CO₂ to light olefins on Cu/Zn_x/(Zn-)SAPO-34 catalysts: Strategy for product distribution. *Fuel* 2019;239:44–52.
- [25] Temvuttiroj C, Chusamboon N, Numpilai T, Faungnawakij K, Chareonpanich M, Limtrakul J, et al. Development of SO₄²⁻-ZrO₂ acid catalysts admixed with a CuO-ZnO-ZrO₂ catalyst for CO₂ hydrogenation to dimethyl ether. *Fuel* 2019;241:695–703.
- [26] Cheng Y-H, Nguyen V-H, Chan H-Y, Wu JCS, Wang W-H. Photo-enhanced hydrogenation of CO₂ to mimic photosynthesis by CO co-feed in a novel twin reactor. *Appl Energy* 2015;147:318–24.
- [27] Khanna N, Fridley D, Zhou N, Karali N, Zhang J, Feng W. Energy and CO₂ implications of decarbonization strategies for China beyond efficiency: modeling 2050 maximum renewable resources and accelerated electrification impacts. *Appl Energy* 2019;242:12–26.
- [28] Mansilla C, Dautremont S, Shoai Tehrani B, Cotin G, Avril S, Burkhalter E. Reducing the hydrogen production cost by operating alkaline electrolysis as a discontinuous process in the French market context. *Int J Hydrogen Energy* 2011;36:6407–13.
- [29] Holladay JD, Hu J, King DL, Wang Y. An overview of hydrogen production technologies. *Catal Today* 2009;139:244–60.
- [30] Turner J, Sverdrup G, Mann MK, Maness PC, Kroposki B, Ghirardi M, et al. Renewable hydrogen production. *Int J Energy Res* 2008;32:379–407.
- [31] Zeng K, Zhang D. Recent progress in alkaline water electrolysis for hydrogen production and applications. *Prog Energy Combust Sci* 2010;36:307–26.
- [32] Rate-based model of the CO₂ capture process by MEA using Aspen Plus. Dataset. Burlington, USA. 2012.
- [33] Li BH, Zhang N, Smith R. Simulation and analysis of CO₂ capture process with aqueous monoethanolamine solution. *Appl Energy* 2016;161:707–17.
- [34] Taqvi SA, Tufa LD, Zabiri H, Mahadzir S, Maulud AS, Uddin F. Rigorous dynamic modelling and identification of distillation column using Aspen Plus. 2017 IEEE 8th Control and System Graduate Research Colloquium (ICSGRC). 2017. p. 262–7.
- [35] Sanchez Fernandez E, Goetheer ELV, Manzolini G, Macchi E, Revzani S, Vlugt TJH. Thermodynamic assessment of amine based CO₂ capture technologies in power plants based on European Benchmarking Task Force methodology. *Fuel* 2014;129:318–29.
- [36] Suhartanto T, York APE, Hanif A, Al-Megren H, Green MLH. Potential utilisation of Indonesia’s Natuna natural gas field via methane dry reforming to synthesis gas. *Catal Lett* 2001;71:49–54.
- [37] Tan LS, Lau KK, Bustam MA, Shariff AM. Removal of high concentration CO₂ from natural gas at elevated pressure via absorption process in packed column. *J Nat Gas Chem* 2012;21:7–10.
- [38] White SP, Allis RG, Moore J, Chidsey T, Morgan C, Gwynn W, Adams M. Natural CO₂ reservoirs on the Colorado plateau and Southern Rocky mountains, USA. A numerical model. 6th International Conference on Greenhouse Gas Control Technologies. Kyoto, Japan. 2003. p. 423–8.
- [39] Kohn MP, Castaldi MJ, Farrauto RJ. Auto-thermal and dry reforming of landfill gas over a Rh/gamma Al₂O₃ monolith catalyst. *Appl Catal B* 2010;94:125–33.
- [40] Ross JRH. Natural gas reforming and CO₂ mitigation. *Catal Today* 2005;100:151–8.
- [41] Ossachoque M, Pompeo F, Gonzalez G. Rh-Ni/CeO₂-Al₂O₃ catalysts for methane dry reforming. *Catal Today* 2011;172:226–31.
- [42] Olah GA, Goepert A, Czaun M, Prakash GKS. Bi-reforming of methane from any source with steam and carbon dioxide exclusively to metgas (CO-2H₂) for methanol and hydrocarbon synthesis. *J Am Chem Soc* 2013;135:648–50.
- [43] Cañete B, Gigola CE, Brignole NB. Enhancing the potential of methane combined reforming for methanol production via partial CO₂ hydrogenation. *Ind Eng Chem Res* 2017;56:6480–92.
- [44] Cañete B, Gigola CE, Brignole NB. Synthesis gas processes for methanol production via CH₄ reforming with CO₂, H₂O, and O₂. *Ind Eng Chem Res* 2014;53:7103–12.
- [45] Lee SG, Sawant A, Rodrigues K, Kulik CJ. Effects of carbon-dioxide and water on the methanol synthesis catalyst. *Energy Fuels* 1989;3:2–7.
- [46] Manenti F, Leon-Garzon AR, Bozzano G. Energy-process integration of the gas-cooled/water-cooled fixed-bed reactor network for methanol synthesis. 16th International Conference on Process Integration, Modelling and Optimisation for Energy Saving and Pollution Reduction. 2013. p. 1243–8.
- [47] Vanden Bussche KM, Froment GF. A steady-state kinetic model for methanol synthesis and the water gas shift reaction on a commercial Cu/ZnO/Al₂O₃ catalyst. *J Catal* 1996;161:1–10.
- [48] Mignard D, Pritchard C. On the use of electrolytic hydrogen from variable renewable energies for the enhanced conversion of biomass to fuels. *Chem Eng Res Des* 2008;86:473–87.
- [49] Carlson EC. Don’t gamble with physical properties for simulations. *Chem Eng Prog* 1996;92:35–46.
- [50] Phair JW, Badwal SPS. Materials for separation membranes in hydrogen and oxygen production and future power generation. *Sci Technol Adv Mater* 2006;7:792–805.

- [51] Amin NAS, Yaw TC. Thermodynamic equilibrium analysis of combined carbon dioxide reforming with partial oxidation of methane to syngas. *Int J Hydrogen Energy* 2007;32:1789–98.
- [52] Song C, Pan W. Tri-reforming of methane: a novel concept for catalytic production of industrially useful synthesis gas with desired H₂/CO ratios. *Catal Today* 2004;98:463–84.
- [53] Abdulrahman AO, Huisings D, Haflamp W. Sustainability improvements in Egypt's oil & gas industry by implementation of flare gas recovery. *J Cleaner Prod* 2015;98:116–22.
- [54] Zhang C, Jun K-W, Gao R, Kwak G, Kang SC. Efficient utilization of associated natural gas in a modular gas-to-liquids process: technical and economic analysis. *Fuel* 2016;176:32–9.
- [55] Zhang C, Jun K-W, Gao R, Kwak G, Park H-G. Carbon dioxide utilization in a gas-to-methanol process combined with CO₂/Steam-mixed reforming: Techno-economic analysis. *Fuel* 2017;190:303–11.
- [56] Zhang C, Jun K-W, Gao R, Lee Y-J, Kang SC. Efficient utilization of carbon dioxide in gas-to-liquids process: Process simulation and techno-economic analysis. *Fuel* 2015;157:285–91.
- [57] Townsend DW, Linnhoff B. Heat and power networks in process design. Part I: criteria for placement of heat engines and heat pumps in process networks. *AIChE J* 1983;29:742–8.
- [58] Townsend DW, Linnhoff B. Heat and power networks in process design. Part II: design procedure for equipment selection and process matching. *AIChE J* 1983;29:748–71.
- [59] Feng X, Berntsson T. Critical COP for an economically feasible industrial heat-pump application. *Appl Therm Eng* 1997;17:93–101.
- [60] Bagajewicz MJ, Barbaro AF. On the use of heat pumps in total site heat integration. *Comput Chem Eng* 2003;27:1707–19.
- [61] Colmenares TR, Seider WD. Heat and power integration of chemical processes. *AIChE J* 1987;33:898–915.
- [62] Rodera H, Bagajewicz MJ. Targeting procedures for energy savings by heat integration across plants. *AIChE J* 1999;45:1721–42.
- [63] Dennis K, Colburn K, Lazar J. Environmentally beneficial electrification: The dawn of 'emissions efficiency'. *Electricity J* 2016;29:52–8.
- [64] Evans A, Strezov V, Evans TJ. Assessment of sustainability indicators for renewable energy technologies. *Renew Sustain Energy Rev* 2009;13:1082–8.
- [65] Schulte Beerbühl S, Fröhling M, Schultmann F. Combined scheduling and capacity planning of electricity-based ammonia production to integrate renewable energies. *Eur J Oper Res* 2015;241:851–62.
- [66] Banares-Alcantara R, Dericks G, Fiaschetti M, Grunewald P, Lopez JM, Tsang E, et al. Analysis of Islanded ammonia-based energy storage systems. Report. University of Oxford; 2015.
- [67] Wang G, Mitsos A, Marquardt W. Conceptual design of ammonia-based energy storage system: system design and time-invariant performance. *AIChE J* 2017;63:1620–37.
- [68] Baronia R, Goel J, Singhal SK. High methanol electro-oxidation using PtCo/reduced graphene oxide (rGO) anode nanocatalysts in direct methanol fuel cell. *J Nanosci Nanotechnol* 2019;19:4315–22.
- [69] Baronia R, Goel J, Gautam G, Singh D, Singhal SK. Synthesis and characterization of nitrogen doped reduced graphene oxide (N-rGO) supported PtCu anode catalysts for direct methanol fuel cell. *J Nanosci Nanotechnol* 2019;19:3832–43.
- [70] Carbon Dioxide Emissions Coefficients by Fuel. Dataset. U.S. Energy Information Administration. 2016.